2014-08

An eddy kinetic energy view of physical and dynamical processes in distinct forecast scenarios for the extratropical transition of two tropical cyclones

An Eddy Kinetic Energy View of Physical and Dynamical Processes in Distinct Forecast Scenarios for the Extratropical Transition of Two Tropical Cyclones*

JULIA H. KELLER+ AND SARAH C. JONES+

Institute for Meteorology and Climate Research (IMK-TRO), Karlsruhe Institute of Technology, Karlsruhe, Germany

PATRICK A. HARR

Department of Meteorology, Naval Postgraduate School, Monterey, California

(Manuscript received 12 July 2013, in final form 18 March 2014)

ABSTRACT

The extratropical transition (ET) of Hurricane Hanna (2008) and Typhoon Choi-Wan (2009) caused a variety of forecast scenarios in the European Centre for Medium-Range Weather Forecasts (ECMWF) Ensemble Prediction System (EPS). The dominant development scenarios are extracted for two ensemble forecasts initialized prior to the ET of those tropical storms, using an EOF and fuzzy clustering analysis. The role of the transitioning tropical cyclone and its impact on the midlatitude flow in the distinct forecast scenarios is examined by conducting an analysis of the eddy kinetic energy budget in the framework of downstream baroclinic development. This budget highlights sources and sinks of eddy kinetic energy emanating from the transitioning tropical cyclone or adjacent upstream midlatitude flow features. By comparing the budget for several forecast scenarios for the ET of each of the two tropical cyclones, the role of the transitioning storms on the development in downstream regions is investigated. Distinct features during the interaction between the tropical cyclone and the midlatitude flow turned out to be important. In the case of Hurricane Hanna, the duration of baroclinic conversion from eddy available potential into eddy kinetic energy was important for the amplification of the midlatitude wave pattern and the subsequent reintensification of Hanna as an extratropical cyclone. In the case of Typhoon Choi-Wan, the phasing between the storm and the midlatitude flow was one of the most critical factors for the future development.

1. Introduction

Several tropical cyclones (TC) per year recurve and start to interact with the midlatitude flow (Evans and Hart 2003, and references therein). This is the prerequisite for the TC to undergo an extratropical transition (ET; Jones et al. 2003). Midlatitude flow characteristics (e.g., stronger wind shear, higher wind speeds) act to accelerate the former TC and trigger its transformation into an extratropical cyclone with the potential for reintensification (Klein et al. 2000, 2002). At the same time, the upper-level outflow of the transitioning TC, together with warm and moist tropical air masses circulating around the system, may have a strong impact on the midlatitude flow configuration.

In several idealized as well as realistic case studies it could be shown that the interaction between the transitioning TC and the midlatitude flow may amplify (e.g., Harr and Dea 2009; Riemer and Jones 2010; Scheck et al. 2011b; Grams 2011), or even trigger (e.g., Bosart and Lackmann 1995; Riemer et al. 2008; Scheck et al. 2011a) the development of a midlatitude Rossby wave train. Hence, the impact of a transitioning TC on the midlatitude flow is not limited to the immediate vicinity of the cyclone itself. The triggered Rossby wave train may propagate far downstream, eventually enhancing the potential for downstream cyclogenesis on the opposite side of the ocean basin (Agustí-Panareda et al. 2004; Harr

* Supplemental information related to this paper is available at the Journals Online website: http://dx.doi.org/10.1175/MWR-D-13-00219.s1.

+ Current affiliation: Deutscher Wetterdienst, Offenbach, Germany.

Corresponding author address: Julia Keller, Deutscher Wetterdienst, Frankfurter Strasse 135, 63067 Offenbach, Germany. E-mail: julia.keller@dwd.de

DOI: 10.1175/MWR-D-13-00219.1

and Dea 2009; Riemer and Jones 2010). The potential for the amplification of a Rossby wave train, as well as for the extratropical reintensification of the former TC depend strongly on the structure of the preexisting flow pattern (Harr and Elsberry 2000; Harr et al. 2000; Klein et al. 2002; Atallah and Bosart 2003) and especially on the relative phasing between the transitioning TC and the midlatitude wave train (McTaggart-Cowan et al. 2001; Ritchie and Elsberry 2003, 2007). If the storm moves ahead of a midlatitude trough, it is in a favorable position for reintensification and its outflow may strongly amplify the adjacent ridge directly east of the storm. Latent heat release in ascending warm air masses ahead of the cyclone (e.g., Bosart and Lackmann 1995; Grams 2011) as well as in the frontal precipitation along the baroclinic zone (Torn 2010) may strongly modulate the potential vorticity (PV) field and thus aid the ridge amplification.

The sensitivity of the ET process to the phasing between the TC and the preexisting midlatitude wave pattern poses a challenge for numerical weather prediction (NWP) systems. Using various ensemble forecast systems, Harr et al. (2008) and Anwender et al. (2008) showed that ET events often coincide with increased forecast uncertainty in downstream regions. By conducting numerical experiments for the ET of Hurricane Helene (1996), Pantillon et al. (2012) further showed how forecast errors associated with the ET event propagate toward downstream regions and lead to increased midrange forecast uncertainty in Europe. Thus, the potential for high-impact weather by the reintensified ex-TC or another cyclone, developing farther downstream, often coincides with poor predictability, which enforces the possible impact of such an event. Reduced predictability can be linked, on the one hand, to a misrepresentation of the influence of the midlatitude flow on the TC, leading to errors in the forecast for structural changes within the TC (Evans et al. 2006) and the acceleration of the system (Jones et al. 2003). On the other hand, reduced predictability can result from the impact of the transitioning storm on the midlatitude flow during the interaction, which may modify the flow configuration. Thus, the improvement of predictability during ET events requires a better understanding of the physical and dynamical processes involved in the interaction between the TC and the extratropical flow, and a revised representation of those processes in numerical weather forecasts.

An adequate framework in which to investigate the amplification and propagation of wave trains is provided by the ''downstream baroclinic development'' paradigm (Orlanski and Sheldon 1995, and references therein). By investigating the distribution of eddy kinetic energy K_e, the deviation of the actual distribution of kinetic energy from a monthly mean state, a wave train stands out as a chain of K_e maxima, associated with the highest wind speeds in the flanks of the troughs and ridges. Advective and dispersive K_e fluxes, together with baroclinic conversion from eddy available potential into eddy kinetic energy then enable investigation of the intensification and downstream propagation of individual K_e maxima and the interaction between neighboring features. The analysis method was already applied successfully to examine the development and amplification of wave patterns in the midlatitudes due to extratropical cyclones (McLay and Martin 2002; Decker and Martin 2005; Cordeira and Bosart 2010). Harr and Dea (2009) used this method and the National Centers for Environmental Prediction (NCEP) Final Analysis (FNL) data for the ET of four typhoons in 2005 to show that a transitioning TC may act as an additional source of K_e, supporting the amplification of midlatitude wave trains. However, the impact on the midlatitude flow and the associated increase in K_e depended strongly on the characteristics of the midlatitude environment, into which the storm moves. Additionally, the ex-TC need not necessarily undergo the whole transition and reintensification process during ET (cf. Klein et al. 2000, 2002) in order to strongly impact the midlatitude flow.

In this work, we will extend the studies from Harr and Dea (2009) to learn more about the distinct processes involved during the interaction between the transitioning cyclone and the midlatitude flow pattern. Instead of using analysis data or deterministic forecasts, which provide one realistic scenario for the ET of a storm, we employ several forecast scenarios from the European Centre for Medium-Range Weather Forecasts (ECMWF) Ensemble Prediction System (EPS; Buizza 2006) for the ET of two TCs. These forecast scenarios indicate multiple ways for how the transitioning storm may interact with the midlatitude flow. By analyzing the K_e budget for these scenarios we get valuable clues to the relative role of the TC and the midlatitude flow configuration during the interaction. In this way, we want to identify the dominant processes during the interaction, describe their representation in the scenarios and thus elucidate their influence on the distinct developments.

After a brief introduction of the analysis technique and the selection of particular ensemble members in the next section, an overview of the two tropical cyclones is provided in section 3. We then analyze the different forecast scenarios for the ET of the two storms using the K_e framework (section 4). Conclusions are drawn in the final section.

TABLE 1. Time on which the two cyclones were declared as extratropical systems, initialization time of the forecasts considered, and time step at which the EOF and cluster analysis was applied, and region over which the EOFs are computed.

Different times	Typhoon Choi-Wan	Hurricane Hanna
ET time	1200 UTC 20 Sep 2009	0600 UTC 7 Sep 2008
Initialization	0000 UTC 15 Sep 2009	0000 UTC 5 Sep 2008
Clustering	0000 UTC 21 Sep 2009	0000 UTC 9 Sep 2008
EOF region	30°–60°N	30°–60°N
	120°–200°E	0°–80°W

2. Data and methods

a. Data

In this study we focus on two ET events with different characteristics and impacts on the midlatitude flow. The first case considered is the ET of Hurricane Hanna (2008), which has had a strong impact on the midlatitude flow (Grams et al. 2011). The other case, the ET of Choi-Wan (2009), was associated with a possible impact on downstream regions, combined with increased forecast uncertainty. For both cases, an ECMWF EPS forecast is employed that was initialized prior to the time, the TC was declared as extratropical by the Regional Specialized Meteorological Center (RSMC; Table 1) and that showed an increase in forecast uncertainty for the 500-hPa geopotential height, directly associated with the ET of the TC (Fig. 1, the red dot marks the position of storm as it was declared extratropical by the RSMC). This increasing forecast uncertainty highlights the impact a transitioning TC may have on the predictability for downstream regions (Anwender et al. 2008; Harr et al. 2008). The strong uncertainty downstream of transitioning Choi-Wan should provide us with clearly distinct development scenarios, whose detailed investigation will then allow us to identify those processes that caused the developments to be different.

Previous studies employing the K_e framework (e.g., Danielson et al. 2004; Decker and Martin 2005; Harr and Dea 2009; Cordeira and Bosart 2010) are based on analysis data, available at 10 and more pressure levels (referred to as vertical output resolution in the remainder). However, data from the operational ECMWF EPS is only available at nine pressure levels. Vertical velocity, which is crucial for the computation of the baroclinic conversion (cf. section 2c), is only available at six pressure levels. This requires determination as to whether the coarse vertical output resolution of the ECMWF EPS forecast data is sufficient to adequately define the K_e budget terms. Based on operational ECMWF Integrated Forecast System (IFS) analysis data (available at 14 pressure levels), we simulated the impact

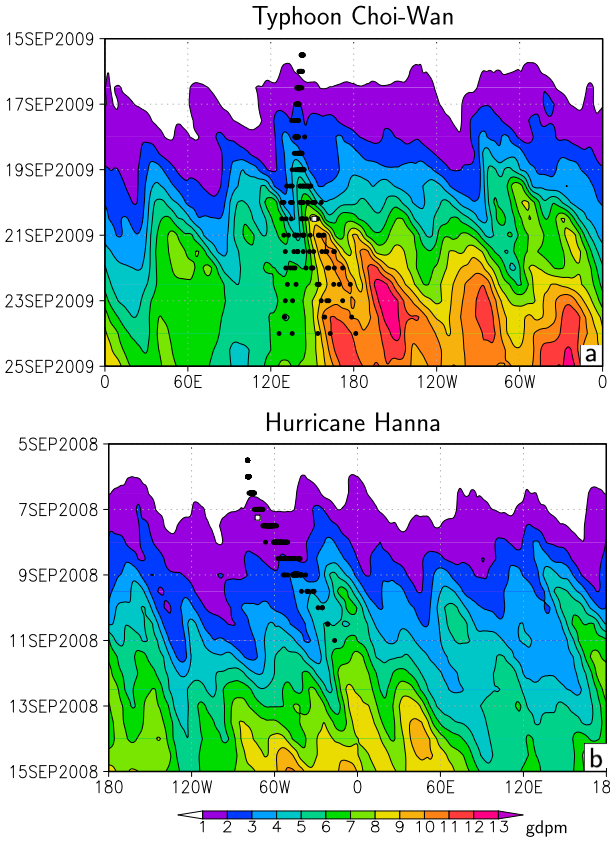

FIG. 1. Standard deviation of 500-hPa geopotential height in the two ECMWF EPS for (a) Typhoon Choi-Wan and (b) Hurricane Hanna averaged between 40° and 60°N. Black dots mark forecast position of surface TC center in the individual ensemble members, white square marks best-track position for ET.

of different vertical output resolutions on the K_e budget terms. In this experiment, the K_e budgets were determined using the vertical resolution of the operational EPS forecasts (six pressure levels for vertical velocity, nine pressure levels for the other quantities), of an experimental setup of the ECMWF EPS (Lang et al. 2012, 10 pressure levels), and the full set of pressure levels from the ECMWF analysis. In this manner, it could be shown that the operational vertical output resolution provides a reasonable definition of the different terms (cf. Keller 2012).

As expected, the largest differences in magnitude and also in spatial distribution were found for baroclinic conversion, but the patterns still represented the key features to be investigated, as stated by an example for Hurricane Hanna (Fig. 2). By comparing the maximum values for baroclinic conversion (numbers in bottom-left corner in Fig. 2) we find that about 93% of the magnitude in the analysis data is reached with the 10-level experimental output resolution, while the maximum

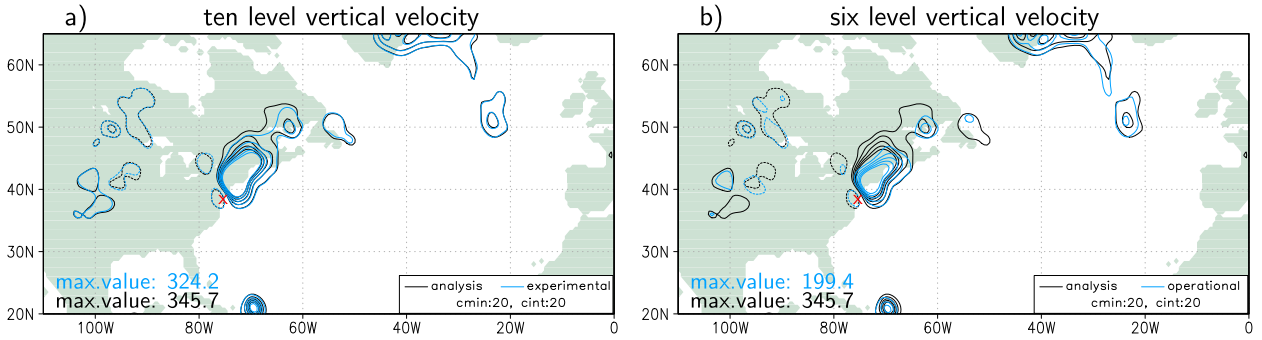

FIG. 2. Baroclinic conversion (in $W m^{-2}$) during the ET of Hurricane Hanna at 0000 UTC 7 Sep 2008 from (a) ECMWF IFS analysis (black) and ECMWF experimental dataset with 10 vertical levels (blue) and (b) ECMWF IFS analysis and ECMWF EPS operational dataset (with 6 vertical levels). The red cross indicates surface position of Hanna. Numbers in bottom-left corner indicate maximum value in each of the datasets. The maximum value of the baroclinic conversion is about 6% lower than the analysis for the experimental data and 42% lower for the operational data.

value in the operational dataset (6 levels) only accounts for 58% of this magnitude. Thus, caution should be exercised when quantitative values of the budget terms, especially of baroclinic conversion, are compared to other studies as the absolute magnitudes in the cases presented here might be smaller than in other studies. In conclusion, an experimental setup of the ECMWF EPS with 10 pressure levels for all variables (Lang et al. 2012) is used for Hurricane Hanna because of the better representation of baroclinic conversion. The forecast for the ET of Choi-Wan is taken from the operational ECMWF EPS as this experimental dataset is not available for this storm. Both are 10-day forecasts, with a 0.5° latitude–longitude resolution and 50 ensemble members.

b. *Identification of forecast scenarios*

To condense the information furnished by the 50 members of the ECMWF EPS, we follow an advanced version of the clustering approach from Harr et al. (2008), which is explained in Keller et al. (2011). We first analyze the empirical orthogonal functions (EOFs) for the atmospheric field under consideration at one specific forecast time and over a region that captures the relevant flow features. This is followed by a fuzzy clustering procedure, applied to the principal components, to extract the main possible development scenarios contained in the forecast. In this study, the method is applied to the 500-hPa geopotential height field and the vertically integrated K_e field, which results in two sets of possible forecast scenarios. However, in most cases these two sets are related to each other, which supercedes a separate investigation of these scenarios. In previous studies (Anwender et al. 2008; Harr et al. 2008; Keller et al. 2011), the development scenarios were examined in terms of the cluster mean. However, as the terms affecting the K_e budget often have a rather limited spatial distribution, averaging over all cluster members would smooth out detailed features of the energy budget. Therefore, we define a representative member for each cluster of the two sets, based on its Euclidean distance to the cluster center for our further investigations. Because of the similarities in the forecast scenarios, some of the 500-hPa geopotential height forecast scenarios share the same representative member with the scenarios, extracted from the K_e field. In these cases, this member could explicitly be defined as representative members. In the other cases we identified the representative member that best resembled the respective cluster mean using the dot product between the field of the representative member and of the cluster mean as a similarity index [more details are provided in Keller (2012)]. The results of our analysis should be related for those members that show likewise contributions to the EOFs, but will start to differ for those members that are located farther away from the cluster means.

c. *Eddy kinetic energy analysis*

In this study we use the K_e equation in pressure coordinates as derived by Orlanski and Katzfey (1991):

$$\frac{\partial K_e}{\partial t} = -\mathbf{v}_h' \cdot \nabla_p \phi' - \nabla_p \cdot (\mathbf{v}_h K_e) - \frac{\partial(\omega' K_e)}{\partial p} - \mathbf{v}_h' \cdot (\mathbf{v}' \cdot \nabla_3 \mathbf{v}_m) + \text{residual}. \quad (1)$$

where ϕ' is the perturbation geopotential, $\mathbf{v}_h$ is the total (horizontal) wind vector, while $\mathbf{v}_m$ defines the mean wind and $\mathbf{v}'$ defines the perturbation or eddy wind; ω' stands for the perturbation vertical velocity. The subscript 3 indicates three-dimensional gradient components. Temporal changes in the local K_e distribution [left-hand side of Eq. (1)] are thus affected by the following quantities:

a generation term describing the work done by pressure forces [first term on right-hand side (rhs)], the horizontal and vertical advection of K_e by the total wind $\mathbf{v}$ (second and third terms on rhs), barotropic interaction between the eddy and the mean flow (fourth term on rhs), and, to a lesser extent, by friction and a second-order correlation term. The latter terms are contained in the residual (Orlanski and Katzfey 1991). More insight into the processes generating K_e via the work done by pressure forces is provided by partitioning the eddy wind in this specific term into a geostrophic and an ageostrophic (subscript a) component. Considering the geostrophic wind in pressure coordinates to be nondivergent, the first term on the rhs of Eq. (1) can be expressed as

$$-\mathbf{v}' \cdot \nabla_p \phi' = -\nabla_p \cdot (\mathbf{v}'_a \phi') - \frac{\partial(\omega' \phi')}{\partial p} + \omega' \alpha' . \qquad (2)$$

The first and second terms on the rhs of Eq. (2) are the horizontal and vertical divergence of the ageostrophic geopotential flux, while the third term is the baroclinic conversion from eddy available potential energy A_e into K_e. The downstream propagation and amplification of wave patterns, as well as the downstream impact of a transitioning TC, can be explained on the basis of the ageostrophic geopotential flux divergence, the divergence of the K_e flux by the total wind, and the baroclinic conversion of K_e. A more detailed explanation of the processes, described by these three quantities is provided in section 3c and in Keller (2012). The barotropic conversion of K_e is involved during the decay of waves, but as it is typically of smaller magnitude (Chang and Orlanski 1993; Decker and Martin 2005), it is not in the focus of our investigations and will be added to the residue.

Following Harr and Dea (2009) the fields are vertically integrated over the available pressure levels (1000–100 hPa) to consider the K_e distribution in the entire troposphere, instead of focusing on one single level only. By normalizing the vertically integrated terms with the gravitational acceleration ($g = 9.81\ \mathrm{m\,s^{-2}}$) the different terms can then be expressed in units resembling the spatial distribution of energy ($\mathrm{J\,m^{-2}}$ for K_e and $\mathrm{W\,m^{-2}}$ for the budget terms). The vertical integration further simplifies Eqs. (1) and (2) as the terms describing the vertical derivations become negligible and the final equation for temporal changes to the local K_e budget reads as

$$\frac{1}{g}\int_{p_s}^{p_t} \frac{\partial K_e}{\partial t} dp = \frac{1}{g}\int_{p_s}^{p_t} [-\nabla_p \cdot (\mathbf{v}'_a \phi') - \omega' \alpha' - \nabla \cdot (\mathbf{v} K_e) + \text{residual}]\, dp , \qquad (3)$$

with the divergence of the ageostrophic geopotential flux (first term rhs), the baroclinic conversion (second term rhs), and the divergence of the K_e fluxes with the total wind (advective flux, third term on rhs). The monthly mean dataset, required for the calculation of the K_e budget, is defined as a 30-day running mean, which is computed from the operational ECMWF IFS analysis, extrapolated on a 0.5° horizontal resolution to remain consistent with the ensemble dataset.

3. Case overview

The two storms under investigation are characterized by distinct life cycles. Both reduced the predictability in downstream regions (Fig. 1) and thus led to the development of clearly distinct forecast scenarios among the ensemble members from the ECMWF EPS. Before considering the different forecast scenarios a brief overview of the observed development is provided.

a. *Typhoon Choi-Wan*

Typhoon Choi-Wan emanated from a tropical depression in the central North Pacific Ocean, which formed around 12 September 2009. Following a predominantly west-northwesterly track over the western North Pacific, the system further intensified to reach a maximum strength of 915 hPa around 16 September 2009. On 18 September 2009, Choi-Wan started to recurve south of Japan and accelerated northeastward into the midlatitudes. At 1200 UTC 19 September 2009 (Fig. 3a), Choi-Wan moved ahead of a preexisting midlatitude trough. Near 42°N, 155°E a frontal wave developed in the vicinity of strong localized precipitation ahead of the transitioning TC. Because of the advection of total column water ahead of Choi-Wan (not shown) this feature perhaps can be characterized as a predecessor rain event (PRE; Galarneau et al. 2010; Schumacher et al. 2011). Around 1200 UTC 20 September 2009, the remnants of Choi-Wan merged with the frontal wave (Fig. 3b) and the merger reintensified strongly as an extratropical cyclone about 24 h later (Fig. 3c). Choi-Wan approached a preexisting and moderately amplified Rossby wave pattern in the midlatitudes. The interaction between the transitioning storm and the midlatitude flow features led to an amplification and modification of the midlatitude Rossby wave train that affected the entire North Pacific. This amplified wave train evolved into a wave breaking event over North America, around 22 September 2009 and the formation of a cutoff cyclone east of the Rocky Mountains. The circulation in the narrowed trough and the cutoff was associated with a temperature drop of about 15–20 K in the western parts of the Great Plains between 21 and 25 September 2009, indicating a significant downstream impact of the transitioning storm.

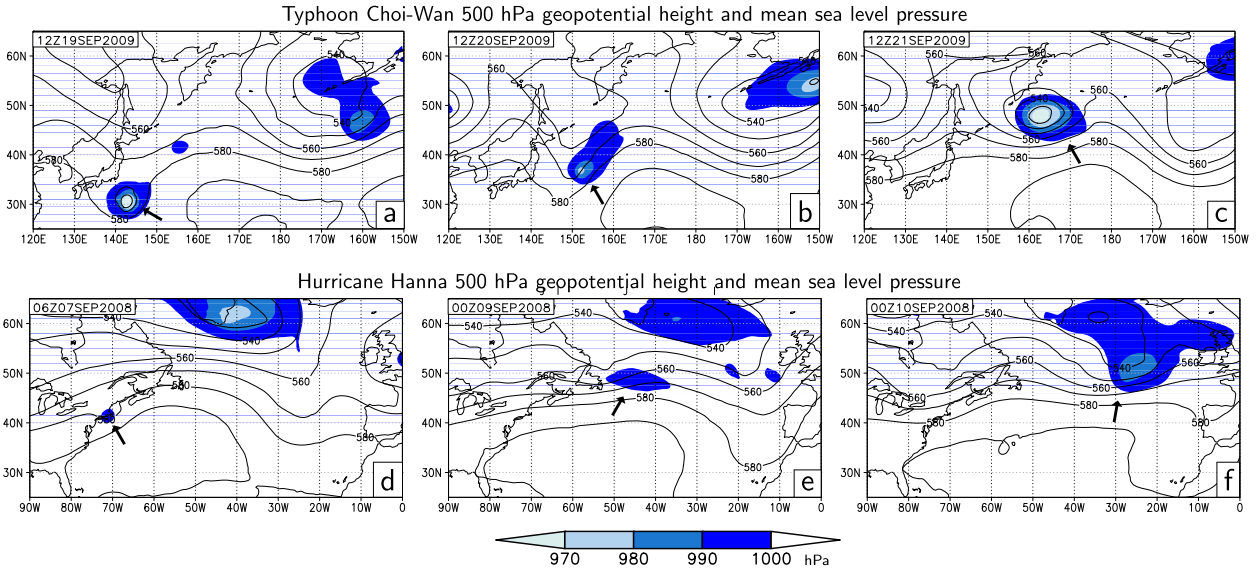

FIG. 3. 500-hPa geopotential height (contours, in gpdm) and mean sea level pressure (shaded, in hPa) from the ECMWF IFS analysis for times indicated in each panel during the extratropical transition of (a)–(c) Typhoon Choi-Wan and (d)–(f) Hurricane Hanna. Arrows indicate storm position.

b. Hurricane Hanna

Hurricane Hanna formed from a tropical wave over the eastern North Atlantic Ocean around 28 August 2008. During its westerly movement toward the Caicos Islands in weak shear, the system intensified to reach hurricane strength around 1 September 2008. After a counterclockwise loop in enhanced environmental shear near Caicos and Haiti, Hanna approached the periphery of the subtropical ridge and accelerated in a northward direction. The storm made landfall near the border between North and South Carolina around 6 September 2008. By 0600 UTC 7 September 2008 (Fig. 3d) Hanna was declared extratropical while moving north-northeastward along the U.S. East Coast to eventually merge with a cold front over southern New England (Brown and Kimberlain 2008). As the system moved offshore just east of Newfoundland, the weakened remnants of ex-Hanna became located ahead of an approaching shortwave trough and reintensified as an extratropical cyclone around 9 September 2008 (Fig. 3e). This system then propagated toward Europe at 0000 UTC 10 September 2008 (Fig. 3f) and eventually supported the formation of a cutoff cyclone in the Mediterranean (Grams et al. 2011).

c. Eddy kinetic energy perspective expressed in Hovmöller diagrams

A more compact overview of the development is provided by the use of Hovmöller diagrams (Hovmöller 1949). Together with the surface position of the storm, the interaction between the midlatitude wave train (in terms of meridional wind at 300 hPa) and the transitioning TC over time becomes obvious (Figs. 4a and 5a). In the ECMWF IFS analysis Choi-Wan directly proceeds into the front flank of a midlatitude trough at 0000 UTC 19 September 2009 (Fig. 4a). This flow configuration is maintained overall until the end of the presented analysis time frame.

Hovmöller diagrams constructed from the component terms of the K_e budget show the distribution of K_e in a wave train and its downstream propagation (e.g., Decker and Martin 2005; Cordeira and Bosart 2010; Glatt et al. 2011). As Hovmöller diagrams form the basis for the remainder of the paper, their interpretation will be briefly explained by considering the K_e together with the meridional wind, the baroclinic conversion, divergence of ageostrophic geopotential flux, and divergence of K_e flux with the total wind [cf. Eq. (3)], derived from the ECMWF IFS analysis for both cases.

In general, the K_e maxima are aligned with regions of highest wind speeds, typically in the flanks of the trough and ridge pattern (Figs. 4a and 5a). The amplification of the individual K_e maxima, and in turn of the wave train, is partially caused by the baroclinic conversion (Fig. 4b) of eddy potential into K_e energy with warm air rising and cold air sinking. In accordance with the conceptual model of ET, developed by Klein et al. (2000), rising warm air in the transitioning Choi-Wan is found in the eastern and northern quadrant of the system, as it moves ahead of the midlatitude trough. In addition, baroclinic conversion is particularly strong in the eastern part of

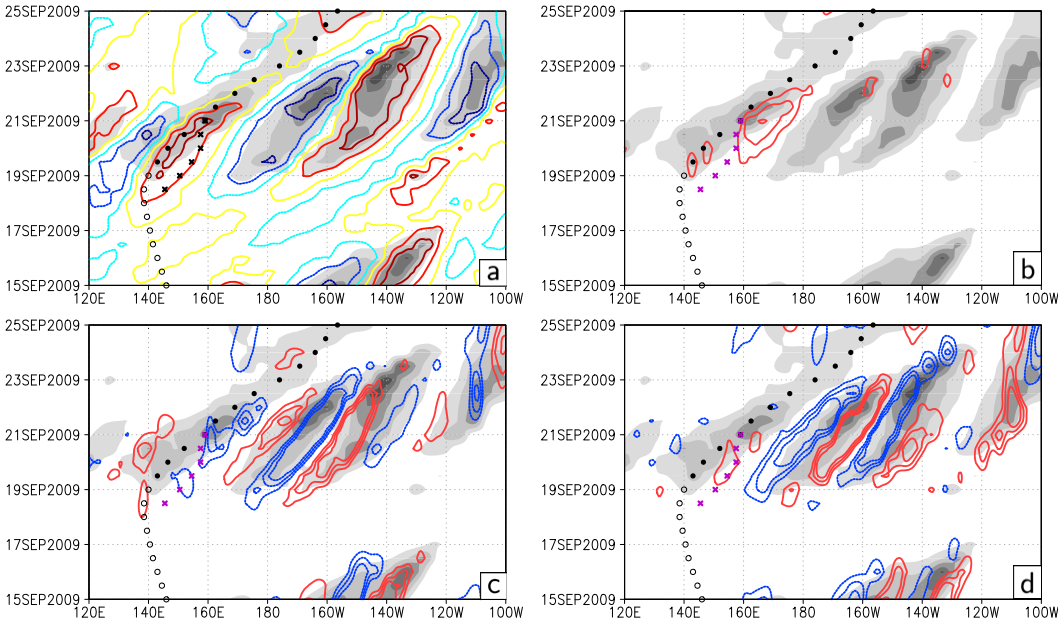

FIG. 4. Hovmöller diagrams for K_e budget terms derived from ECMWF IFS analysis for Typhoon Choi-Wan (averaged between 30° and 60°N). (a) Vertically averaged K_e (shaded, in 10, 15, 20, 25, and 30×10^5 J m^{-2}, cf. Fig. 8) and meridional wind (contours, southerly wind in warm, northerly wind in cool colors, every 5, 15, and 25 m s^{-1}). (b) Vertically averaged K_e and baroclinic conversion of K_e (contours, every 15, 25, and 35 W m^{-2}). (c) Vertically averaged K_e and divergence of ageostrophic geopotential flux (contours, every 15, 25, and 35 W m^{-2}, blue: divergence, red: convergence). (d) Vertically averaged K_e and divergence of K_e flux with the total wind (contours, every 15, 25, and 35 W m^{-2}, blue: divergence, red: convergence). Surface position of each TC marked as a dot, filled when storm is within latitude belt for averaging. The × marks surface position of the extratropical cyclone. Wave trains for Choi-Wan are marked by dashed lines.

the K_e maximum, slightly ahead of the front flank of the upstream trough (Fig. 4b, 1200 UTC 19 September–0000 UTC 20 September) and is thus associated with rising warm air along the baroclinic zone near the frontal wave. As Choi-Wan and the extratropical system merge (0000 UTC 21 September), the generation of K_e via baroclinic conversion continues. Diverging and converging ageostrophic geopotential fluxes (Fig. 4c) disperse eddy kinetic energy via work done by pressure forces between adjacent K_e maxima and thus steer the propagation of the entire wave packet (group velocity). Typically, the ageostrophic geopotential flux is divergent (blue contours) in the eastern part or exit region of the K_e maximum, and convergent (red contours) in the western part or entrance region (Fig. 4c). In case of dominant converging fluxes, the K_e maximum grows, while dominant diverging fluxes act as a sink of K_e and may even cause the decay of the K_e maxima, when the entire K_e is dispersed into the adjacent downstream maximum (Orlanski and Sheldon 1995). Strong downstream dispersion of K_e occurs near the merger of Choi-Wan and the frontal wave (Fig. 4c). It partly superposes the region of baroclinic conversion, indicating the downstream dispersion of this newly generated K_e. The divergence and convergence of the K_e flux by the total wind mainly acts to redistribute K_e within an individual K_e maxima. Flux divergence in the eastern and convergence in the western part of the maxima (Fig. 4d) redistributes energy from the entrance to the exit region and leads to an eastward propagation of the individual K_e maxima (phase velocity). This process is clearly evident for wave train w_a in the case of Choi-Wan (Fig. 4d).

Hurricane Hanna first proceeds into a midlatitude ridge and aligns with the shortwave trough later (around 1200 UTC 10 September 2008, Fig. 5a). Baroclinic conversion is strong in the eastern and northern quadrant of the TC as the system approaches the midlatitude flow and moves along the U.S. East Coast (Fig. 5b). Along the way, baroclinic conversion decreases (after 0000 UTC 8 September 2008) but is maintained until Hanna becomes positioned ahead of the shortwave midlatitude trough (partly below contour interval in Fig. 5b). Divergence of the ageostrophic geopotential flux is strong at the beginning and K_e from the vicinity of the storm is partly dispersed northward (not shown) and downstream into the adjacent ridge (until 0000 UTC 8 September 2008, between 90° and 30°W), but does not propagate farther eastward through the North Atlantic. This downstream

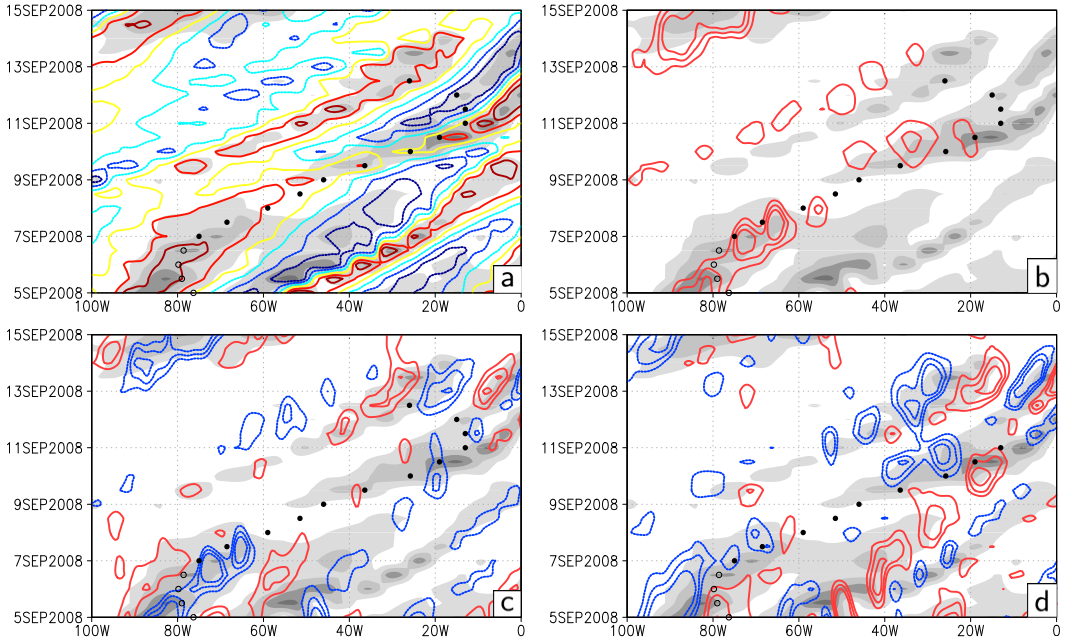

FIG. 5. As in Fig. 4, but for ECMWF IFS analysis for Hurricane Hanna (averaged between 40° and 55°N).

dispersion of K_e ceases to exist before Hanna reintensifies as an extratropical cyclone. During the reintensification, ageostrophic geopotential fluxes recirculate within Hanna (not shown) and downstream dispersion remains weak (Fig. 5c). Divergence and convergence patterns, resembling advection of the entire K_e maxima can also be identified in this case (Fig. 5d).

4. Results for the distinct forecast scenarios

a. Forecast scenarios for Typhoon Choi-Wan

To further examine the impact of Choi-Wan on the midlatitude flow we chose an ECMWF EPS forecast that was initialized well before the actual ET (cf. Table 1) and that was characterized by strongly increasing forecast uncertainty, in association with Choi-Wan (Fig. 1). As all members forecast the recurvature of Choi-Wan into the midlatitudes, the forecast uncertainties were related to the interaction of the TC with the midlatitude flow and not to uncertainty about the recurvature of the storm (Anwender et al. 2008). The geopotential height EOFs (Figs. 6a,b) and the EOFs of K_e (not shown) capture the position and amplitude of the tropical cyclone (TY) and of the downstream wave pattern (T1, T2). Four clusters were extracted for each forecast scenario set, with well distributed members and contributions to the EOFs (Table 2). Thereby, the scenarios extracted from the 500-hPa geopotential height EOFs and the K_e EOFs were related to each other, two of them have the same representative members. We chose those four representative members that best resemble the cluster means and show clearly distinct developments (Keller 2012). For one scenario the representative member of the K_e-based clustering is chosen instead of the representative member of geopotential height clustering, as it captures the characteristic development of this cluster to a better extent. The K_e budget for several scenarios provides information on the factors responsible for the different developments.

1) SCENARIO I

In scenario I, Choi-Wan moves toward a rather weakly amplified midlatitude trough near Japan and becomes embedded close to its center (Fig. 8a). A slight frontal wave develops northeast of Choi-Wan in association with this trough (Fig. 7a). However, the large-scale midlatitude flow is dominated by a trough over the central to eastern North Pacific, resembling the northeast circulation pattern during ET (Harr et al. 2000). Later in the forecast (after 0000 UTC 22 September 2009), the frontal wave and its associated shortwave trough replace the former central to eastern North Pacific trough, intensify without any interaction with the transitioning storm and propagate into the Gulf of Alaska (Fig. 8).

A moderate maximum of K_e characterizes Choi-Wan between 19 and 21 September 2009 (Fig. 8c), while no clear K_e maximum can be identified around the frontal wave. The baroclinic conversion, associated with the transitioning storm as well as with the frontal wave (Fig. 8c) is rather weak. At the same time, diverging ageostrophic

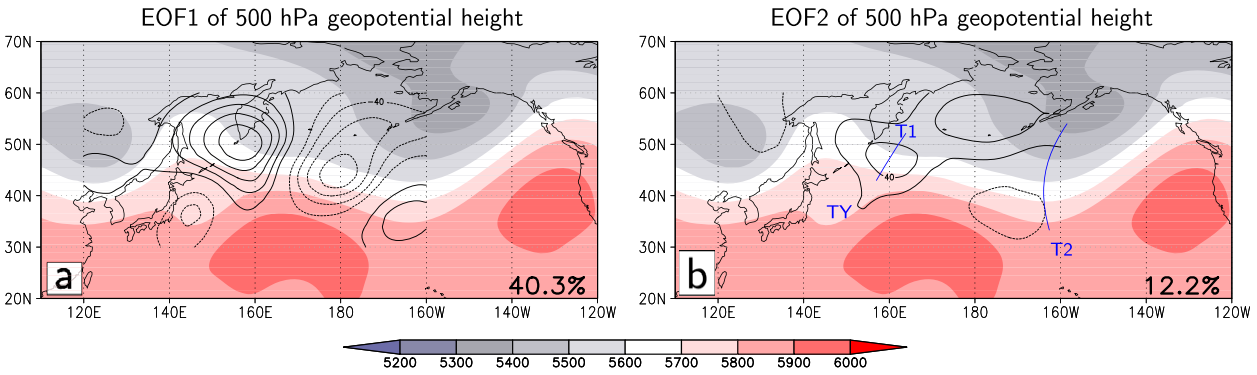

FIG. 6. (a) EOF1 and (b) EOF2 for 500-hPa geopotential height (contours, in gpm, positive: solid, negative: dashed) and ensemble mean of 500-hPa geopotential height (shaded, in gpm) for Typhoon Choi-Wan (TY) at investigation time (0000 UTC 21 Sep 2009, cf. Table 1). Percentage of uncertainty, captured by the respective EOF is given at bottom right. Blue lines indicate axes of troughs T1 and T2.

geopotential fluxes act to disperse some K_e from Choi-Wan into the midlatitude trough over Japan, as the outflow of the storm moves down the geopotential gradient, and farther downstream into the dominant central North Pacific depression (Fig. 8e, between 19 and 21 September 2009, east of 140°E). Converging ageostrophic geopotential fluxes emanating from upstream regions provide additional energy to the maximum associated with the transitioning TC (divergence and convergence dipole between 120° and 140°E, 20 September 2009). Later, the upstream support is maintained until Choi-Wan weakens (not shown), but the downstream dispersion drops completely. Overall, baroclinic conversion, as well as the downstream dispersion and advection of K_e (Fig. 8g) is rather weak in this scenario, suggesting that Choi-Wan has only a minor impact on the downstream development.

2) SCENARIO II

The midlatitude trough over Japan in scenario II is stronger and Choi-Wan stays longer in the front flank of the trough before moving toward the trough center (Fig. 8b, 17–19 September 2009 and Fig. 7b) than in scenario I. Although the downstream trough in the central to eastern North Pacific is established as in scenario I, the stronger trough over Japan leads to the scenario resembling the northwestern circulation pattern from Harr et al. (2000). The frontal wave is embedded in the fore flank of the trough and much closer to Choi-Wan than in scenario I. Around 20 September, Choi-Wan and the frontal wave start to rotate around each other and eventually merge on 21 September 2009 to form a strong extratropical cyclone. This cyclone then propagates eastward, embedded in the center of the trough, and eventually forms a cutoff in the central North Pacific.

At the onset of interaction around 1200 UTC 19 September, the TC and frontal wave are characterized by separated maxima of K_e (Figs. 8d and 10c). They merge into a single dominant maximum associated with the established extratropical cyclone (Fig. 8d, after 1200 UTC 20 September 2009). Between 0000 UTC 19 September and 1200 UTC 20 September 2009, strong baroclinic conversion is connected with the northern quadrant of Choi-Wan and especially with the southern part of the baroclinic zone, extending southeastward from the frontal wave (Figs. 8d and 11a). In this region, warm air ascents along the baroclinic zone, partially driven by the anticyclonic circulation of the subtropical ridge, and frontogenesis along a warm front takes place. The direct thermal circulation of the transitioning TC is responsible for the ascent of warm air northeast and north of Choi-Wan. Some energy support from the upstream trough over central Russia via converging ageostrophic geopotential fluxes is evident between 18 and 20 September 2009 (Fig. 8f). Diverging ageostrophic geopotential fluxes first emanate from the frontal wave between 0000 UTC 19 September and 1200 UTC

TABLE 2. Results of the cluster analysis for the geopotential height and K_e EOFs for Typhoon Choi-Wan. Cluster (column 1), number of members (column 2), contribution of cluster center to EOF1 and EOF2 of the geopotential height or K_e field (columns 3 and 4, respectively), and scenario they represent in this study (column 5). Representative members under investigation are from the clusters marked in boldface font.

Cluster	No. of members	Contribution to EOF1	Contribution to EOF2	Scenario
GPH 1	11	−0.30	1.30	
GPH 2	9	0.39	−1.30	III
GPH 3	14	0.18	0.65	I
GPH 4	10	−1.61	0.21	II
K_e **1**	11	−0.30	1.37	IV
K_e 2	5	1.94	−0.22	
K_e 3	11	−0.14	−0.88	
K_e 4	14	−0.58	−0.14	

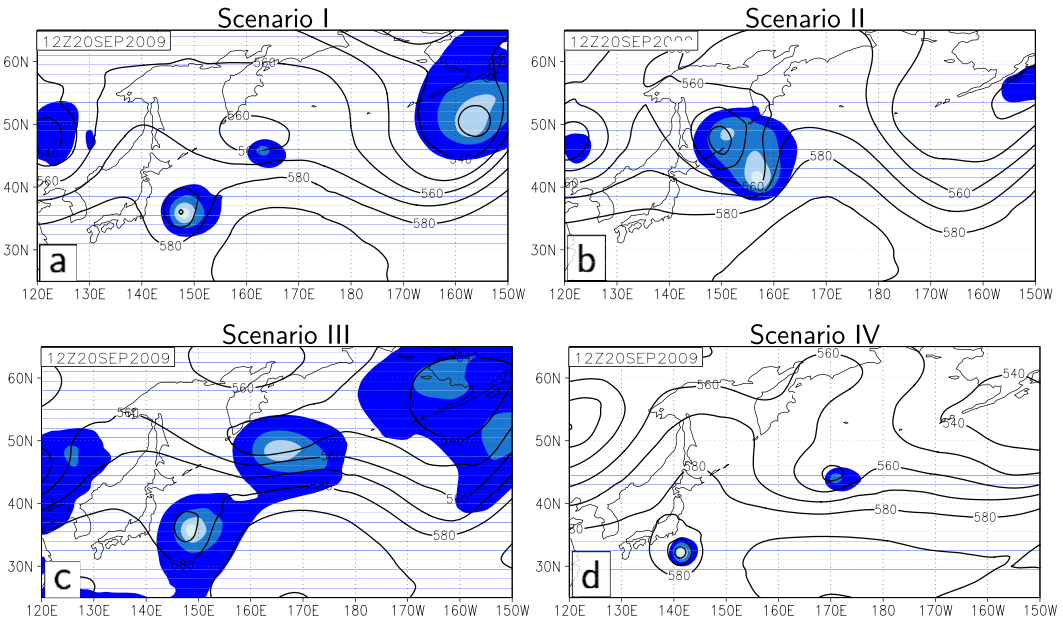

FIG. 7. 500-hPa geopotential height (contours, in gpdm) and mean sea level pressure (shaded, in hPa) for the four forecast scenarios for Typhoon Choi-Wan at 0000 UTC 20 Sep 2009, after onset of interaction between Choi-Wan and the midlatitude flow. Shading as in Fig. 3.

20 September, and later from the merged system as the upper-level outflow crosses toward increasing heights (Fig. 8f). These dispersive energy fluxes converge in the energy maximum of the downstream trough at around 170°E–180° and thus clearly support the amplification of the adjacent ridge and the subsequent downstream wave pattern. Between 19 and 21 September 2009 and 140°–160°E, K_e is advected (Fig. 8h) from Choi-Wan (divergence) into the midlatitude trough near Japan (convergence). This flux convergence is superimposed with diverging ageostrophic geopotential fluxes. Hence, it is evident that Choi-Wan acts as an additional source of K_e, supporting the amplification of the downstream wave pattern. The strong downstream dispersion of K_e by the ageostrophic geopotential flux then causes the merged system to weaken around 22 September 2009, which is manifested in a decreasing magnitude of the associated K_e center. Subsequently, the weakening is partially slowed down by additional gain of energy from upstream regions as defined by converging dispersive energy fluxes between 22 and 23 September 2009 and 140°–160°W (Fig. 8f). Around 23 September 2009, energy fluxes associated with the merged system start to recirculate within the K_e maxima and the downstream support ceases completely. However, energy fluxes from upstream regions still act as an additional source and maintain the K_e maximum, until the merger cuts off in the central North Pacific. Therefore, in scenario II Choi-Wan phases with the midlatitude circulation such that a strong downstream response is forced.

3) SCENARIO III

In the third scenario Choi-Wan moves ahead of a moderately amplified upper-level trough, but is located closer to the trough axis as in scenario II. The extratropical flow is, as in scenario I, dominated by a downstream trough northeast of Choi-Wan (Fig. 9a). The frontal wave is more strongly amplified and already farther away from Choi-Wan than in the other scenarios (Fig. 7c). It then connects to the dominant system in the central and eastern North Pacific and separates quickly from the transitioning storm. The ridge, which was originally located northwest of Choi-Wan, passes the transitioning storm to its north during the subsequent forecast days. Around 23 September 2009, Choi-Wan is then located on the rear flank of the ridge, while the total extratropical flow becomes more zonal toward the end of the forecast time.

Maxima of K_e are associated with both systems (Figs. 9c and 10d). Between 19 and 20 September 2009, K_e is generated via baroclinic conversion in the vicinity of the transitioning cyclone (Fig. 9c, 145°–150°E) as well as ahead of the frontal wave (Fig. 9c, 155°–160°E). The energy maximum associated with Choi-Wan is strongly augmented by converging ageostrophic geopotential fluxes from upstream regions (Figs. 9e and 10d), but also loses some energy because of diverging energy fluxes ahead of the storm. The frontal wave also disperses K_e farther downstream, which only slightly converges in the

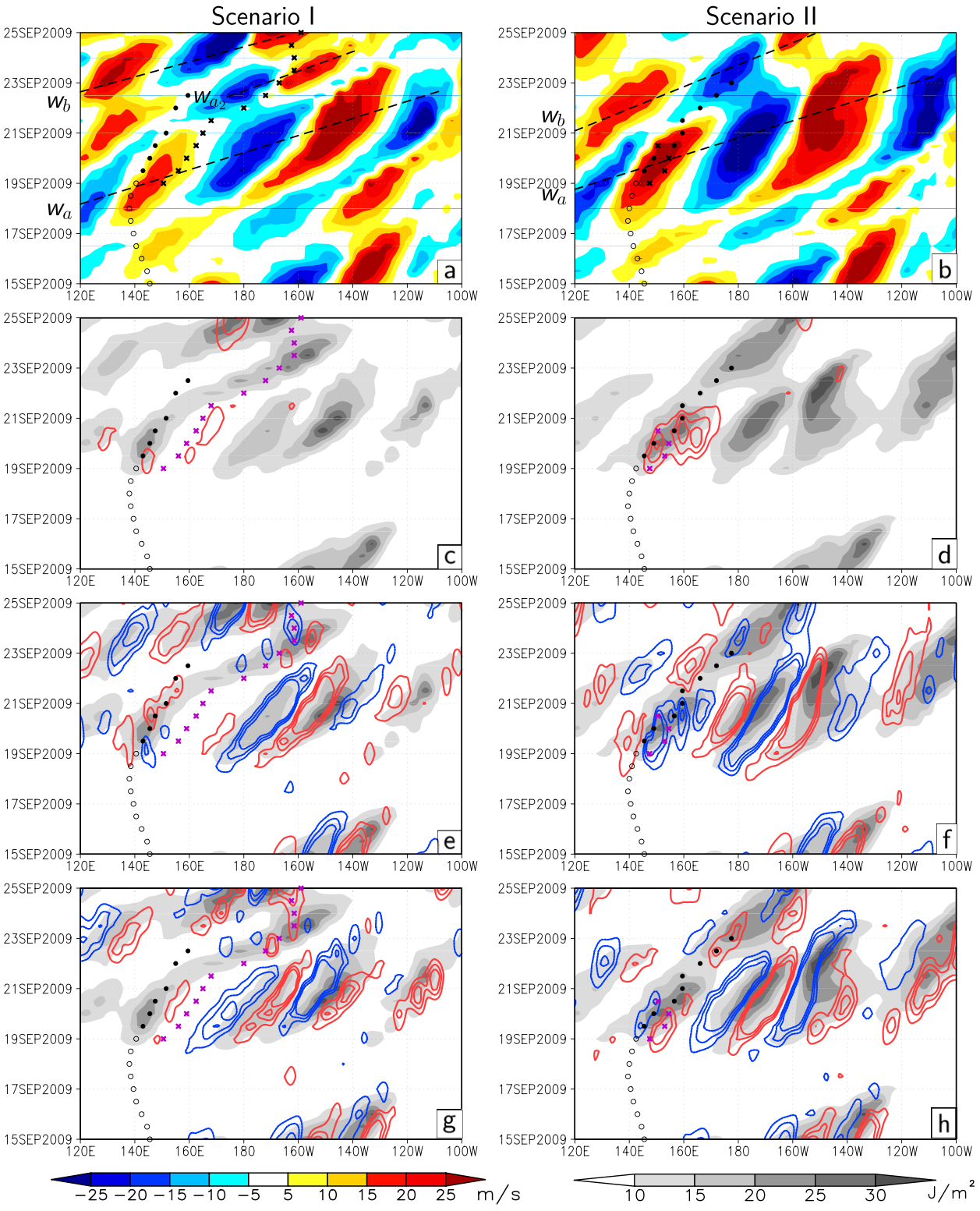

FIG. 8. Hovmöller diagrams for (left) scenario I and (right) scenario II for the ET of Typhoon Choi-Wan. (a),(b) Meridional wind (units for these and all other terms and labels as in Fig. 4). (c),(d) Vertically averaged K_e and baroclinic conversion of K_e. (e),(f) Vertically averaged K_e and divergence of ageostrophic geopotential flux. (g),(h) Vertically averaged K_e and divergence of the advection of K_e with the total wind.

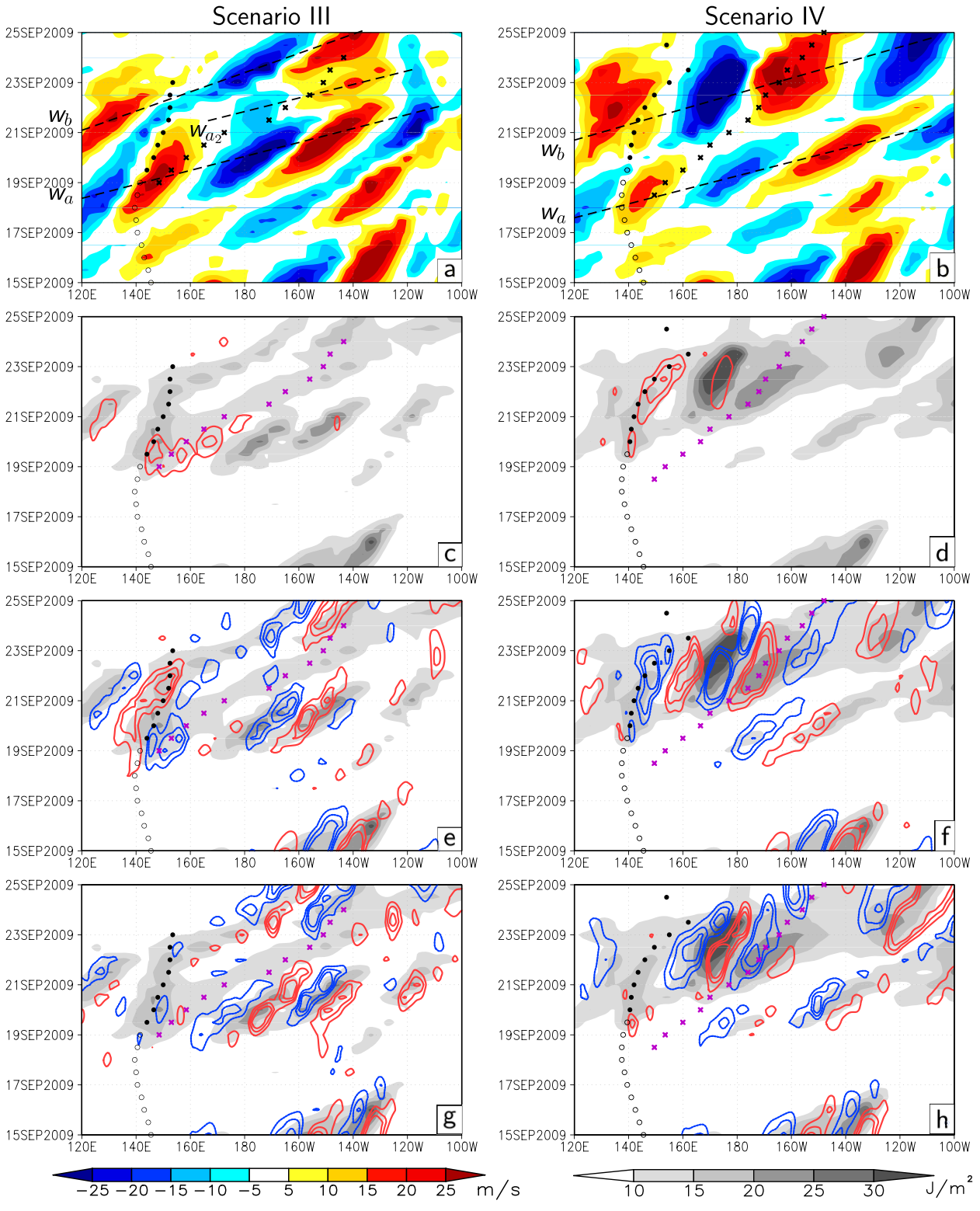

FIG. 9. As in Fig. 8, but for scenario III and IV for the ET of Typhoon Choi-Wan.

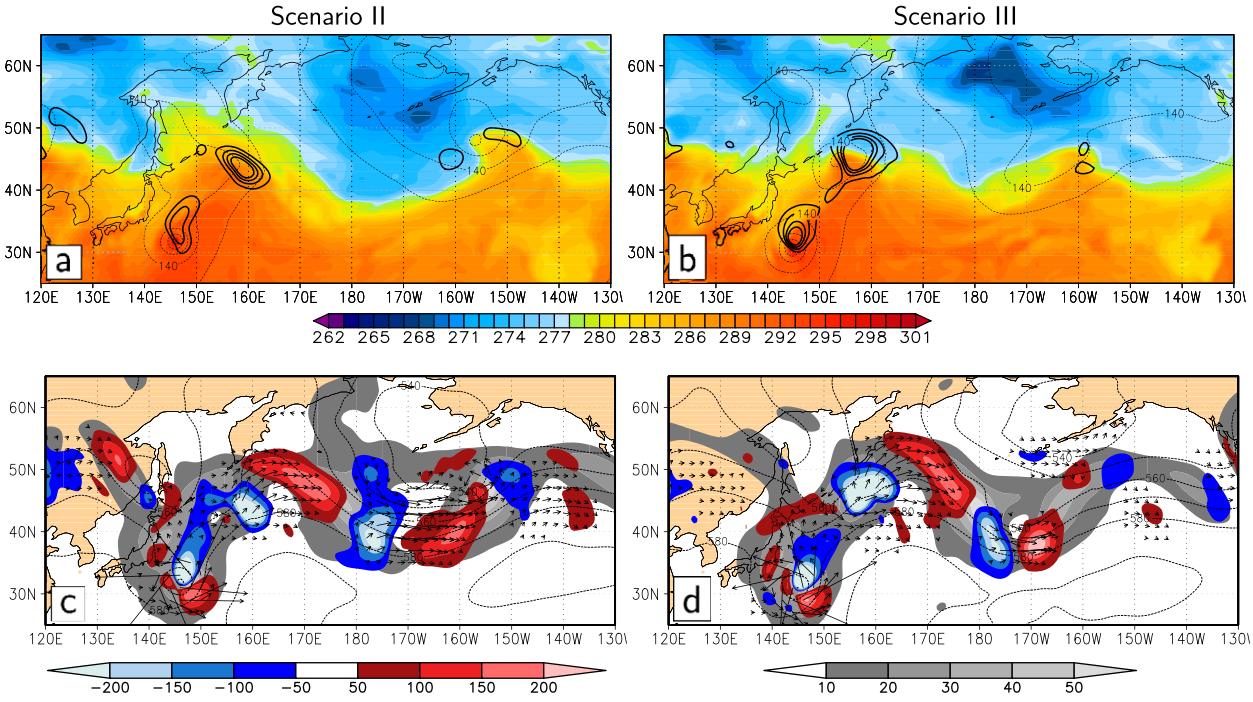

FIG. 10. (left) Scenario II and (right) scenario III for Typhoon Choi-Wan at 1200 UTC 19 Sep 2009. (a),(b) 850-hPa geopotential height (dashed contours, in gpdm), 850-hPa temperature (shaded, in K), and vertically averaged baroclinic conversion (thick black contours, dashed when negative, every 50, 100, 150, and 200 W m^{-2}). (c),(d) Vertically averaged K_e (shaded, in 10^5 J m^{-2}), ageostrophic geopotential flux (arrows, in 10^6 W m^{-1}), divergence of flux (shaded, in W m^{-2}), and 500-hPa geopotential height (dashed contours, in gpdm).

energy maxima, associated with the downstream trough. Additionally, the total wind advects K_e away from the transitioning cyclone toward the frontal wave around 20 September 2009 (Fig. 9g). Hence, Choi-Wan apparently supports the K_e maximum associated with the frontal wave. As the ridge passes the transitioning storm to its north, the baroclinic conversion as well as the cross-contour flow and thus the ageostrophic geopotential flux are suppressed, while the upstream energy maxima still disperses energy toward the transitioning cyclone. With this, the downstream support emanating from Choi-Wan stops completely. Baroclinic conversion ahead of the frontal wave is maintained (Fig. 9c) as the system traverses through the central North Pacific. Toward the end of the forecast the frontal wave is positioned ahead of a trough. Although some energy fluxes emanate from the transitioning cyclone during the initial interaction, the downstream impact of Choi-Wan is rather weak in this scenario, leading to a weaker amplification of the downstream wave pattern. However, comparatively strong energy fluxes from upstream midlatitude regions maintain the energy maxima, associated with Choi-Wan for quite some time.

4) SCENARIO IV

A contrasting development is found in this scenario as Choi-Wan moves into the center of a strongly amplified and dominant ridge over Japan (Fig. 7d) and remains in the western North Pacific for quite a long time (Fig. 9b, between 19 and 21 September 2009). Around 21 September 2009 a moderately amplified trough approaches the remnants of the cyclone from upstream, erodes the dominant ridge and brings the storm into a more favorable position for possible reintensification. The frontal wave is located ahead of the subsequent downstream trough and propagates eastward rather quickly, separating itself from Choi-Wan. Later in the forecast (around 22 September 2009), the remnants of the tropical cyclone become a boundary feature of a slightly intensifying extratropical cyclone, embedded ahead of the upstream trough.

While a clearly identifiable K_e maximum is associated with Choi-Wan (Fig. 9d), the frontal wave is rather weakly amplified and does not have a clear energy maxima. Because of the weak baroclinicity in the ridge, the generation of K_e via baroclinic conversion is only weak during the first days of interaction (Fig. 9d, 19–21 September 2009) and only minor dispersive energy fluxes emanate from the transitioning storm before 20 September 2009. The weak baroclinic conversion also hinders a further amplification of the K_e maxima. As the upstream trough slightly approaches the ex-TC around 21 September 2009, the baroclinicity is enhanced and strong generation of K_e

via baroclinic conversion within the transitioning cyclone is initiated (Fig. 9d, 21–23 September 2009). At the same time, this region is superimposed by strongly diverging ageostrophic geopotential fluxes (Fig. 9f), which disperse the newly generated K_e through and over the crest of the ridge toward the dominant trough in the central North Pacific. This baroclinic conversion and downstream dispersion of K_e continues, while the remnants of Choi-Wan merge with an extratropical depression ahead of the upstream trough. Hence, in this fourth scenario Choi-Wan also clearly acts as an additional source of K_e, supporting the amplification of the downstream wave pattern. However, the downstream support is initiated at a later stage of the forecast, when the transitioned storm becomes positioned ahead of the midlatitude upstream trough.

5) A MORE DETAILED VIEW ON SCENARIOS II AND III

At the onset of interaction, the patterns of baroclinic conversion in scenario II and III resemble each other in appearance. Nevertheless, their developments differ strongly in the course of the forecast. These differences can be traced back to distinct interactions between Choi-Wan and the midlatitude flow. Around 1200 UTC 19 September 2009, Choi-Wan and the frontal wave are more separated from each other in scenario III than in scenario II (Figs. 10a,b). Baroclinic conversion in scenario II occurs in regions with weaker temperature gradients and is not as strong as in scenario III, especially in the region of the frontal wave. In scenario II the low-level temperature shows a broad ridge that expands northward, while the temperature gradient in scenario III is modulated by short waves with less northward dilatation. Important differences are also found for the height structure of the midlatitude flow and the position of Choi-Wan with respect to the trough axis (Figs. 10c,d). Choi-Wan is still located ahead of the nearly upright upstream trough and thus in a favorable setting for further reintensification in scenario II. In this position, its upper-level outflow may aid the amplification of the adjacent downstream ridge and decelerate the eastward propagation of the trough. In scenario III, the upstream trough axis is aligned in a more northeast–southwest orientation. Its southern portion is already in the process of cutting off. Its northern portion is more mobile, has passed Choi-Wan, and brings the frontal wave in a favorable position for further intensification. Overall, the midlatitude flow becomes more zonal in this scenario, supporting the fast eastward translation of the frontal wave during the next few days. Ageostrophic geopotential fluxes recirculate within Choi-Wan, while showing no strong dispersion of K_e into the midlatitudes in either of the scenarios. In contrast, strong downstream dispersion of K_e is associated with the frontal wave in both cases.

Choi-Wan and the frontal wave merge until 1200 UTC 20 September 2009 in scenario II, and strong baroclinic conversion occurs at the baroclinic zone along the prominent ridge directly downstream of Choi-Wan (Fig. 11a). The region of strong baroclinic conversion is superimposed by diverging ageostrophic geopotential fluxes. These fluxes converge in the K_e maximum of the downstream trough, illustrating the impact of the merger of Choi-Wan and the frontal wave on the midlatitude flow (Fig. 11c). In scenario III, the midlatitude baroclinic zone shows a rather zonal alignment, and baroclinic conversion has decreased. The frontal wave veers away from Choi-Wan (Fig. 11b). Dispersive fluxes recirculate K_e within the frontal wave and only weak downstream dispersion occurs. In addition, K_e is dispersed from Choi-Wan into the K_e maximum of the frontal wave (Fig. 11d). Furthermore, a dipole pattern of divergence and converging fluxes is found along the western flank of the K_e maximum, associated with Choi-Wan, indicating an additional energy support from upstream regions.

Horizontal plots for scenarios I and IV are provided in the online supplemental material for completeness.

6) THE IMPACT OF CHOI-WAN ON THE MIDLATITUDE WAVE TRAIN

According to the results presented above, the ET of Choi-Wan had a strong impact on the amplification of the midlatitude wave pattern during and after the ET event. In the analysis (Fig. 4a) a strong amplification of the wave train directly downstream of the ET event (marked as w_a) began at 17 September 2009 and affected the entire northern Pacific basin during the following week. At around 23–25 September 2009 another, but less amplified wave train can be observed to propagate eastward, emanating from upstream regions (marked as w_b). If Choi-Wan proceeds into a northeastern circulation pattern and does not merge with the extratropical system (scenario I and III), wave train w_a developing directly downstream of the ET event becomes only moderately amplified (Figs. 8a and 9a). Toward the end of the forecast, wave train w_b also develops in those scenarios. However, in between these two wave trains, a secondary trough–ridge pattern (w_{a_2}) develops in association with the extratropical cyclone, veering away from Choi-Wan and the inherent generation of K_e due to baroclinic processes. In these cases, Choi-Wan has only a minor impact on the amplification of the wave train w_a. Furthermore, converging energy fluxes from upstream regions suggest a midlatitude forcing in scenario III. If Choi-Wan merges with the frontal wave (scenario II, Fig. 8b), wave train w_a is strongly amplified, due to the

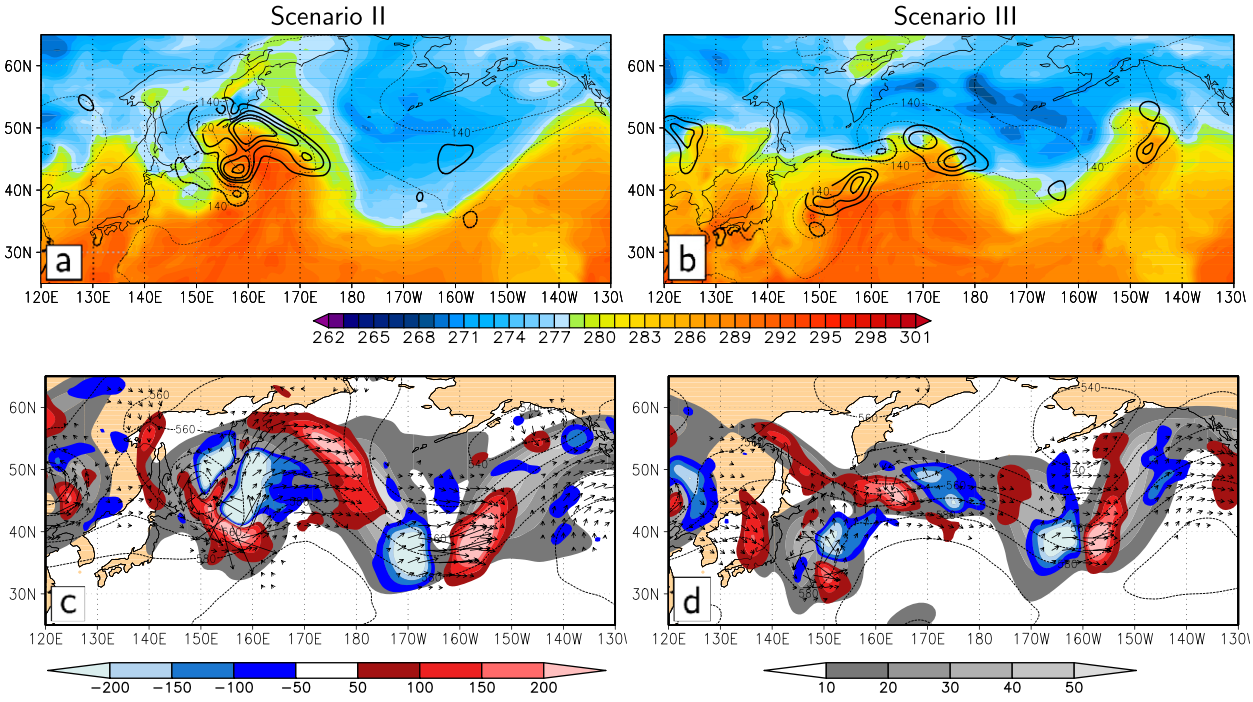

FIG. 11. As in Fig. 10, but for 1200 UTC 20 Sep 2009.

downstream dispersion of K_e, emanating from the storm, and propagates farther downstream as in the analysis dataset. In addition, the development of wave train w_b can be observed in this scenario as well, while no clear signature of the w_{a_2} wave train is identifiable. In the final scenario, where Choi-Wan first proceeds into the ridge over Japan, which hindered the downstream dispersion of K_e out of Choi-Wan, the wave train w_a is amplified only slightly (Fig. 9b). Later in the forecast, the energy fluxes emanating from Choi-Wan help to strongly amplify the second wave train, which was supposed to become wave train w_b of the analysis dataset.

b. *Forecast scenarios for Hurricane Hanna*

For Hurricane Hanna we chose a forecast that was initialized rather close to ET (cf. Table 1) and therefore all members contained the recurvature of the storm, but showed an increase in uncertainty downstream of the ET event (Fig. 1). The EOFs for Hurricane Hanna (Figs. 12a,b) are associated with the position of an incipient trough east of Newfoundland (T1) and the amplitude and alignment of the downstream trough (T2) west of Europe. The K_e EOFs capture related features (not shown). Four clusters were extracted for each forecast scenario set with a slightly different number of members and positive as well as negative contributions to EOF1 and -2 (Table 3). However, despite differences in the spatial and especially temporal development, three of the four scenarios in both sets were related to each other in showing a reintensification of the transitioning storm as an extratropical cyclone and the amplification of the midlatitude wave pattern. Only one of the four scenarios was clearly distinct from the others. Hence, only two of the four scenarios will be considered in the remainder of this work, one with and one without the reintensification of Hanna. From the three related scenarios we chose the one that showed the most intense reintensification. Both scenarios result from the geopotential height clustering (Keller 2012) but closely resemble scenarios found in the K_e clustering. During the early forecast period, the two scenarios for the ET of Hanna partially capture the observed development. Strongest differences occur for the representation of landfall and the detailed structure of the midlatitude wave pattern. An analysis of the K_e budget indicates the reasons for the distinct developments in the course of the forecast.

1) SCENARIO I

The rather weak remnants of Hanna (in terms of surface pressure, not shown) in the first scenario recurve, become embedded in a moderately amplified trough and move over land along the East Coast of the United States (Fig. 13a). Around 8 September 2008, a slight shortwave trough approaches Hanna from upstream (Fig. 14a). This trough develops into a broad, but moderately amplified central North Atlantic trough, while the remnants of

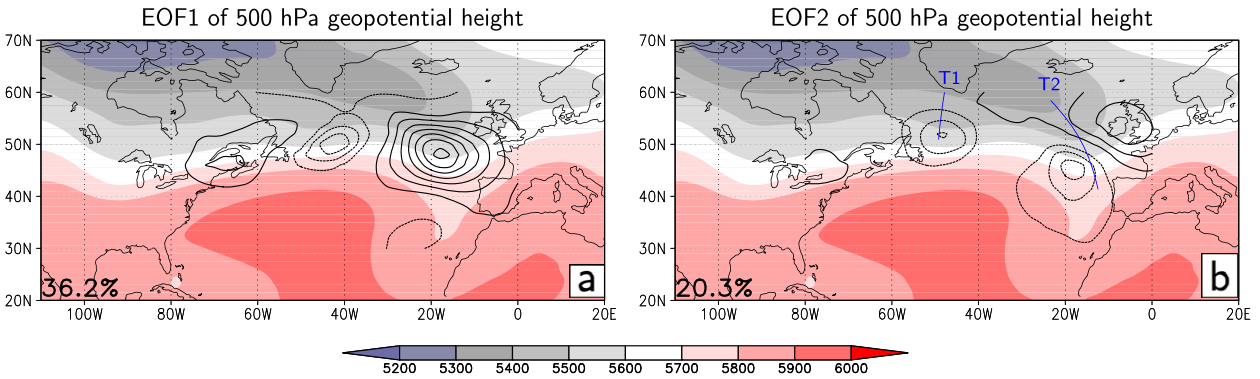

FIG. 12. (a) EOF1 and (b) EOF2 for 500-hPa geopotential height (contours, in gpm, positive: solid, negative: dashed) and ensemble mean of 500-hPa geopotential height (shaded, in gpm) for Hurricane Hanna at investigation time (0000 UTC 9 Sep 2008, cf. Table 1). Percentage of uncertainty captured by the respective EOF is given at bottom left. Blue lines indicate axes of troughs T1 and T2.

Hanna are still embedded in its front flank and thus in a favorable position for further reintensification. The remnants of the tropical cyclone reintensify and reach Europe as a moderately amplified extratropical cyclone.

As the interaction begins, energy maxima are associated with the transitioning cyclone and expand along the midlatitude wave pattern (Fig. 13c). However, rather weak baroclinic conversion of K_e is associated with Hanna during the early forecast days (Fig. 13c). Instead, comparatively strong baroclinic conversion occurs along a baroclinic zone that expands northeastward of Hanna. At the same time, this region coincides with diverging ageostrophic geopotential fluxes that disperse K_e into the downstream wave train (Fig. 13e until 8 September 2008). The baroclinic conversion (Fig. 13c) within the baroclinic zone lasts until the remnants of the transitioning tropical cyclone start to interact with the shortwave trough and begin to reintensify (Fig. 14c). Strong baroclinic conversion is then initiated within the transitioning cyclone itself. The energy fluxes start to recirculate within the energy maximum ahead of the trough, instead of dispersing the newly generated K_e into the downstream wave pattern (Fig. 15). This interplay between energy generation via baroclinic processes and recirculating energy fluxes help to amplify the former shortwave depression into a dominant trough. In turn, this aids the reintensification of Hanna. At the same time, the lack of energy fluxes, emanating from the transitioning storm, hampers the further amplification of the downstream wave pattern, where K_e decreases (Fig. 13e). Eventually, the reintensified ex-Hanna moves toward Europe and leads to the development of a Mediterranean cyclone, in accordance with the analyzed development (not shown). During the entire forecast, the advection of K_e with the total wind mainly acts to redistribute energy within the maxima (Fig. 13g).

2) SCENARIO II

The remnants of the transitioning TC are somewhat stronger (surface pressure, not shown) in scenario II and recurve ahead of a slightly weaker amplified midlatitude wave. In this scenario the TC just clips the U.S. coast (Fig. 13b). In the medium range of the forecast (9–12 September 2008) a rather zonal flow is established over the entire North Atlantic basin. A very weak shortwave disturbance approaches the transitioning cyclone from upstream (Fig. 14b) with no interaction and thus no amplification of the flow features occurs in this case. Thus, the midlatitude wave pattern remains rather weakly amplified, until an upstream trough approaches from the west at later forecast time (after 12 September 2008). Weak remnants of Hanna are caught up by an inchoate shortwave trough around 1200 UTC 10 September 2008,

TABLE 3. Results of the cluster analysis for the geopotential height and K_e EOFs for Hurricane Hanna. Cluster (column 1), number of members (column 2), contribution of cluster center to EOF1 and EOF2 of the geopotential height or K_e field (columns 3 and 4, respectively), and scenario they represent in this study (column 5). Representative members under investigation are from the clusters marked in boldface font.

Cluster	No. of members	Contribution to EOF1	Contribution to EOF2	Scenario
GPH 1	7	−0.93	1.38	I
GPH 2	13	−0.32	−0.00	
GPH 3	12	1.24	0.11	
GPH 4	8	−0.47	−1.38	II
K_e 1	16	−0.80	−0.09	
K_e 2	4	0.10	−0.89	
K_e 3	9	1.78	−0.14	
K_e 4	14	−0.01	1.57	

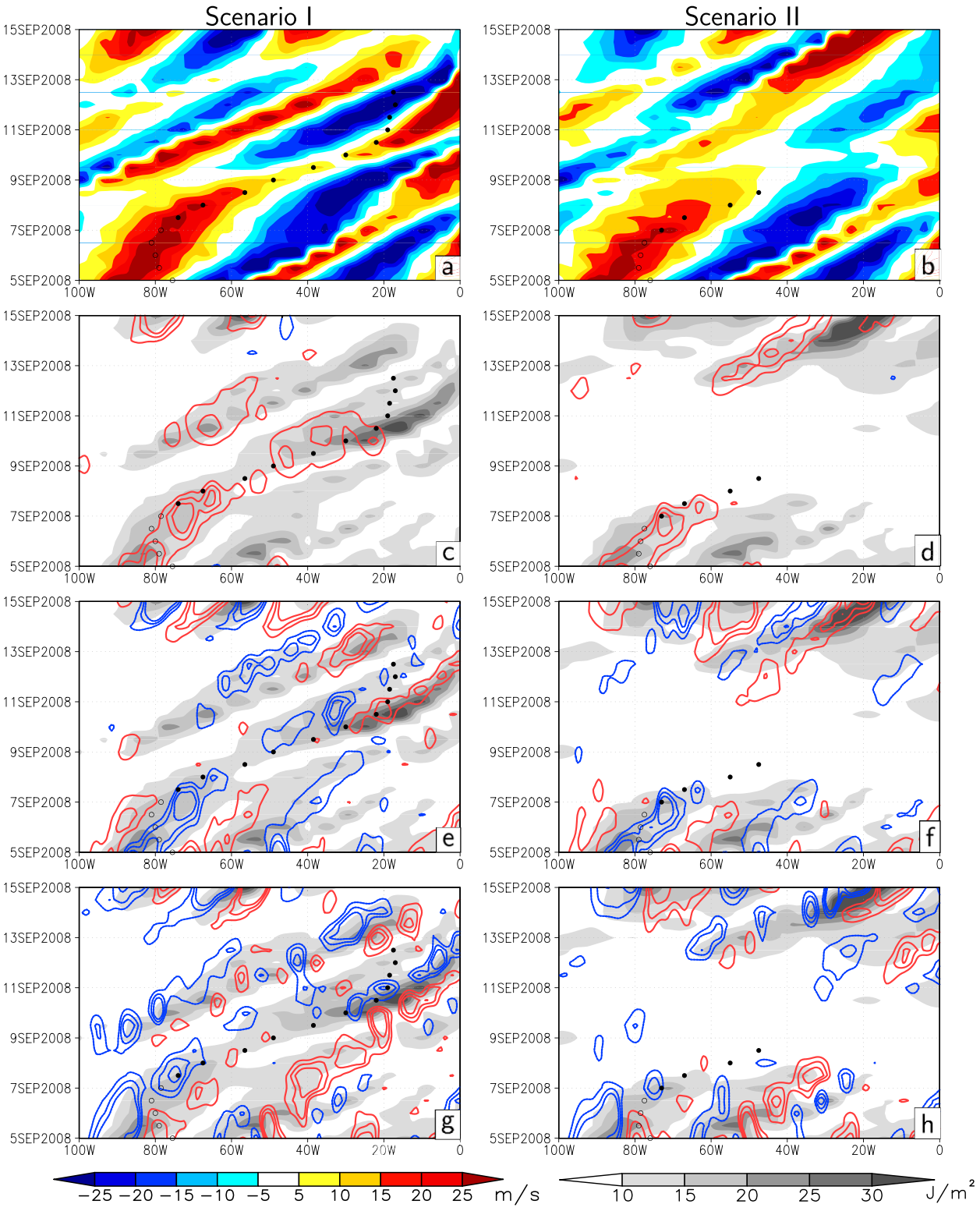

FIG. 13. Hovmöller diagrams for (left) scenario I and (right) scenario II for the ET of Hurricane Hanna (2008). (a),(b) Meridional wind (these and all other terms as in Fig. 4). (c),(d) Vertically averaged K_e and baroclinic conversion of K_e. (e),(f) Vertically averaged K_e and divergence of ageostrophic geopotential flux. (g),(h) Vertically averaged K_e and divergence of advective flux of K_e with the total wind.

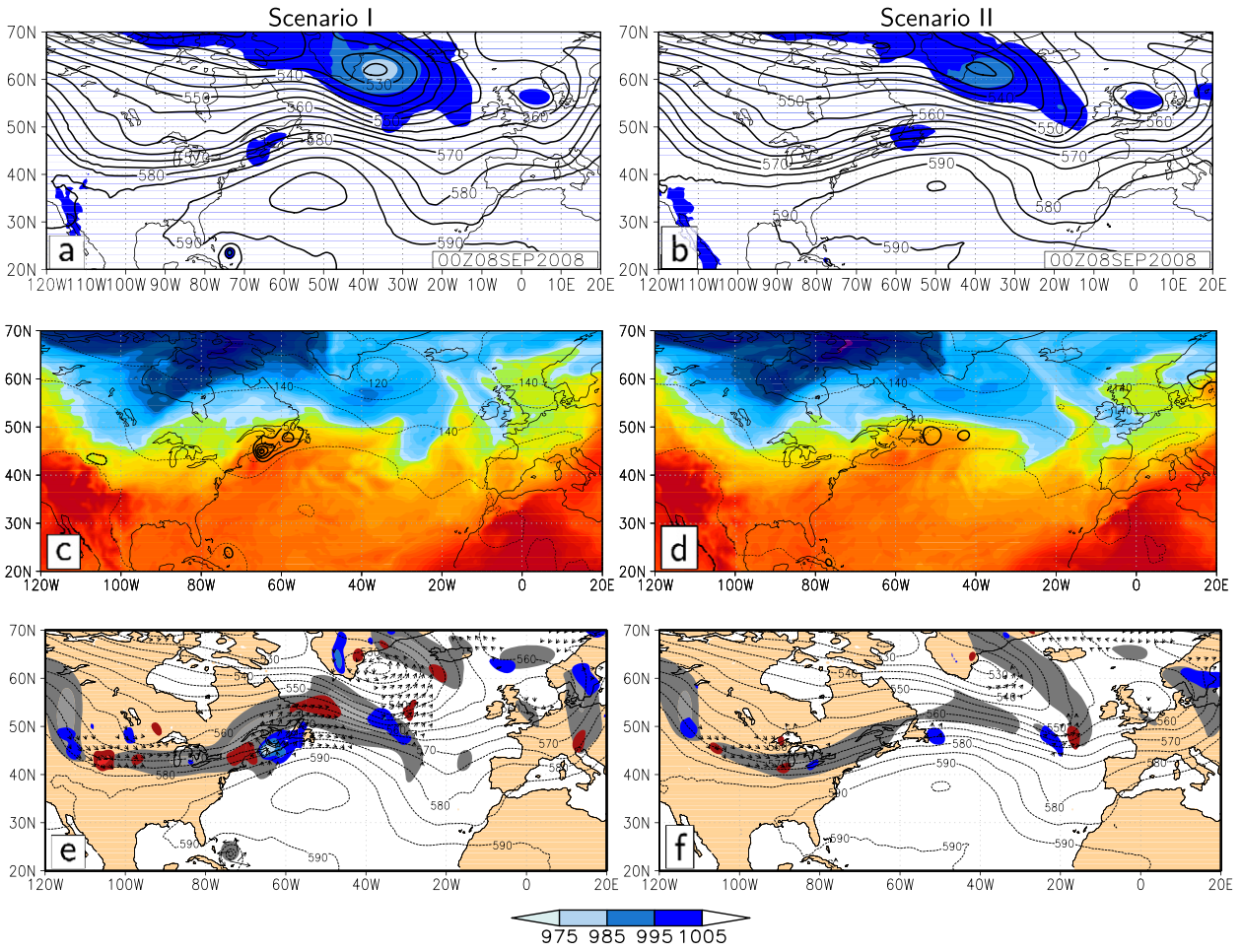

FIG. 14. Scenario I and II for Hurricane Hanna at 0000 UTC 8 Sep 2008. (a),(b) 500-hPa geopotential height (contours, in gpdm) and mean sea level pressure (shaded, in hPa, note difference in shading intervals to Fig. 3). (c),(d) 850-hPa geopotential (dashed contours, in gpdm), 850-hPa temperature (shaded, in K), and vertically averaged baroclinic conversion (thick black contours, dashed when negative, every 50, 100, 150, and 200 $W m^{-2}$). (e),(f) Vertically averaged K_e (shaded, in $10^5 J m^{-2}$), ageostrophic geopotential flux (arrows, in $10^6 W m^{-1}$), divergence of flux (shaded, in $W m^{-2}$), and 500-hPa geopotential (dashed contours, in gpdm). Other shading intervals as in Fig. 10.

but then move toward Europe as a slightly open wave without any reintensification.

Clearly identifiable K_e maxima are associated with the remnants of Hanna and the adjacent midlatitude trough (Fig. 13d). Strong baroclinic conversion occurs in the northern portion of the transitioning cyclone and is dominant about the energy generation along the baroclinic zone (Fig. 13d, Hanna is located within the maximum on 7 September 2008). However, this newly generated energy in the vicinity of Hanna is directly dispersed into the downstream midlatitude wave pattern by diverging ageostrophic geopotential fluxes, crossing toward higher heights (Fig. 13f). It is worth noting that the distribution of diverging and converging ageostrophic geopotential fluxes is nearly similar in both scenarios, although slightly time shifted. The baroclinic conversion within the extropical cyclone then stops almost completely (Fig. 13d, 8 September 2008 and later) before the shortwave disturbance approaches (Fig. 14d). Furthermore, the associated energy center is already weakened (Fig. 14f), because of the former downstream dispersion of K_e. Because of the missing generation of additional K_e, the shortwave trough is not amplified further and the remnants of Hanna decay. Even as the remnants are absorbed by another shortwave trough toward the end of the forecast, no gain of K_e and thus no reintensification occurs. Advective fluxes redistribute K_e within the maxima at the beginning but also drop almost completely as the remnants of Hanna decay (Fig. 13h).

5. Conclusions

Different physical and dynamical processes play an important role during the interaction between tropical

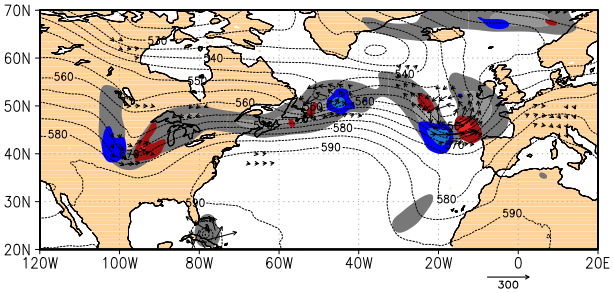

FIG. 15. Scenario I for Hurricane Hanna at 0000 UTC 9 Sep 2009. Vertically averaged K_e (shaded, in 10^5 J m^{-2}), ageostrophic geopotential flux (arrows, in 10^6 W m^{-1}), divergence of flux (shaded, in W m^{-2}), and 500-hPa geopotential (dashed contours, in gpdm). Shading intervals as in Fig. 10.

cyclones undergoing ET and the midlatitude flow. As it was shown in a previous study (Harr and Dea 2009), analysis of the K_e budget provides a framework in which the impact of the transitioning storm on the midlatitude flow can be examined. In the present work we have expanded the use of the K_e budget for several forecast scenarios for the ET of two tropical cyclones extracted from ECMWF EPS forecasts. By comparing the energy budget of the distinct forecast scenarios, contained in the ensemble, key processes were identified as causes of the diverging developments.

In the case of Typhoon Choi-Wan (2009), four distinct forecast scenarios could be identified. In these scenarios, the impact of Choi-Wan on the extratropical flow depended strongly on the position of the transitioning storm relative to a preexisting midlatitude trough–ridge couplet over Japan and an associated frontal wave southeast of Kamchatka. As Choi-Wan moved into a favorable position ahead of the midlatitude trough (scenario II), strong baroclinic conversion due to the thermal circulation of the transitioning cyclone and the ascent along the baroclinic zone produced additional K_e. This K_e was dispersed into the downstream wave pattern by the ageostrophic geopotential flux. The transitioning cyclone merged with the frontal wave and the systems reintensified as a moderately amplified extratropical cyclone with ongoing energy dispersion into the downstream wave pattern. Choi-Wan and its associated baroclinic conversion provided an additional source of K_e supporting the amplification of the downstream wave pattern (Harr and Dea 2009). If Choi-Wan propagated toward the center of the midlatitude trough and is positioned farther away from the frontal wave, some baroclinic conversion and downstream dispersion of kinetic energy might exist during the beginning of the ET event (scenario III). However, the downstream support emanating from the transitioning cyclone toward the frontal wave ceased to exist, as this system moved away along with the central North Pacific trough to undergo amplification independent of the TC. If the frontal wave was well separated from Choi-Wan even in the beginning of the ET process, weak baroclinic conversion and downstream dispersion was associated with Choi-Wan (scenario I). This caused a negligible impact of Choi-Wan on the midlatitude flow. In scenario IV, Choi-Wan propagated into a dominant ridge over Japan, which first hindered strong baroclinic conversion within the transitioning cyclone. As this ridge eroded and the remnants of Choi-Wan interacted with another extratropical cyclone approaching ahead of an upstream trough, strong baroclinic conversion and diverging ageostrophic geopotential fluxes initiated the impact of Choi-Wan on the downstream wave train. This development partially resembled the findings from Harr and Dea (2009) for the ET of Typhoon Banyan (2005). In the case of Banyan, energy generation and dispersion did not become established until the already transitioned ex-tropical cyclone had reintensified as an extratropical cyclone. The duration of the downstream impact of Choi-Wan in the several scenarios seems to be limited to a rather short period of about 1–2 days. Thereafter, the downstream dispersion of K_e nearly ceased to exist, although the remnants of Choi-Wan might still have been strong (e.g., scenario II). This suggests that the midlatitude flow is sensitive to the impact of a transitioning cyclone for a limited time frame. The impact of Choi-Wan on the amplification of the downstream wave pattern and on the development of high-impact weather events in downstream regions will be further addressed in a subsequent publication.

During the ET of Hurricane Hanna the differences in baroclinic conversion could be clearly identified as the significant cause of the distinct developments. While the baroclinic conversion and downstream dispersion in the vicinity of Hanna was weaker in scenario I at the beginning of the interaction, it lasted until the remnants of Hanna moved ahead of a shortwave trough. Recirculating energy fluxes and the ongoing baroclinic conversion then aided the further amplification of the associated trough and the reintensification of Hanna as an extratropical cyclone. In scenario II, baroclinic conversion was already stronger during the onset of interaction, as was the downstream dispersion. However, the energy generation ceased to exist and the maximum weakened before the remnants became positioned ahead of an inchoate shortwave disturbance. This lack of K_e then impeded an amplification of the trough as well as the associated reintensification of Hanna. Although the two scenarios were related in the beginning, the final outcome differs strongly. Keeping in mind the differences in flow configuration, this coincides with the findings of Klein et al.

(2002) who showed that slight displacements had major impacts in how the TC interacted with the midlatitude flow and led to large changes in the downstream patterns. The crucial role of baroclinic conversion of K_e is in accordance with previous studies of the ET of Hurricane Hanna. By applying potential vorticity (PV) inversion, along with trajectory calculations, Grams et al. (2011) showed that cross-isentropic airflow that resembled warm conveyor belts caused the north and northeastward ascent of low-PV air in the vicinity of the transitioning storm. The ascending air originated from the inner core as well as from the northern and eastern sector of Hanna, and ascended along a baroclinic zone to the north. This low-PV air was the decisive factor for the amplification of the ridge, developing just east of Hanna, and the subsequent downstream wave pattern. Furthermore, latent heat release within the transitioning cyclone caused the production of new PV in the low and midlevels, supporting the reintensification of Hanna as an extratropical cyclone. Concomitantly, the stronger ridge amplification also strengthened the upstream trough, approaching from North America. Although we could not resolve individual airflows with our analysis method, the importance of ascending warm air masses is manifested in the strong and ongoing baroclinic conversion and thus fit nicely with the results of Grams et al. (2011). Harr and Dea (2009) also identified that baroclinic conversion of K_e due to rising warm air predominantly in the eastern half of the transitioning cyclone was in accordance with the conceptual model of Klein et al. (2000) and provided an additional source of K_e to support amplification of the downstream wave pattern.

To further assess the impact of a tropical storm on the midlatitude flow it is also necessary to expand knowledge, gained from case studies to a more general framework. The results obtained by examining only six specific development scenarios can be expanded by conducting ensemble sensitivity studies to further highlight the dependencies between the TC and the development in the midlatitudes. Correlations between processes associated with energy fluxes that emanate from the transitioning storm and the amplification of the downstream ridge are expected to give further indications on the important processes during an ET event.

Acknowledgments. This study was supported by the German Research Council (DFG) as part of research unit PANDOWAE (FOR 896). The contribution of Patrick Harr was supported by NSF Grant ATM-0736003. We are grateful for constructive comments and suggestions from two anonymous reviewers. We thank Edmund Chang for important advice on the analysis method. Valuable comments and suggestions from Jason Cordeira, Heather Archambault, and Christian Grams helped to improve the manuscript significantly. Access to ECMWF data was provided via the special project ''spdeet.'' We also thank Simon Lang for providing the experimental ECMWF EPS runs.

REFERENCES

Agustí-Panareda, A., C. D. Thorncroft, G. C. Craig, and S. L. Gray, 2004: The extratropical transition of Hurricane Irene (1999): A potential vorticity perspective. *Quart. J. Roy. Meteor. Soc.,* **130,** 1047–1074, doi:10.1256/qj.02.140.

Anwender, D., P. A. Harr, and S. C. Jones, 2008: Predictability associated with the downstream impacts of the extratropical transition of tropical cyclones: Case studies. *Mon. Wea. Rev.,* **136,** 3226–3247, doi:10.1175/2008MWR2249.1.

Atallah, E. H., and L. F. Bosart, 2003: The extratropical transition and precipitation distribution of Hurricane Floyd (1999). *Mon. Wea. Rev.,* **131,** 1063–1081, doi:10.1175/1520-0493(2003)131<1063:TETAPD>2.0.CO;2.

Bosart, L. F., and G. M. Lackmann, 1995: Postlandfall tropical cyclone reintensification in an weakly baroclinic environment: A case study of Hurricane David (September 1979). *Mon. Wea. Rev.,* **123,** 3268–3291, doi:10.1175/1520-0493(1995)123<3268:PTCRIA>2.0.CO;2.

Brown, D. P., and T. Kimberlain, 2008: Tropical Cyclone Report Hurricane Hanna (AL082008), 28 August–7 September 2008. National Hurricane Center, 36 pp. [Available online at http://www.nhc.noaa.gov/pdf/TCR-AL082008_Hanna.pdf.]

Buizza, R., 2006: The ECMWF ensemble prediction system. *Predictability of Weather and Climate,* T. Palmer, and R. Hagedorn, Eds., Cambridge University Press, 459–488.

Chang, E. K. M., and I. Orlanski, 1993: On the dynamics of a storm track. *J. Atmos. Sci.,* **50,** 999–1015, doi:10.1175/1520-0469(1993)050<0999:OTDOAS>2.0.CO;2.

Cordeira, J. M., and L. F. Bosart, 2010: The antecedent large-scale conditions of the Perfect Storms of late October and early November 1991. *Mon. Wea. Rev.,* **138,** 2546–2569, doi:10.1175/2010MWR3280.1.

Danielson, R. E., J. R. Gyakum, and D. N. Straub, 2004: Downstream baroclinic development among forty-one cold-season eastern North Pacific cyclones. *Atmos.–Ocean,* **42,** 235–250, doi:10.3137/ao.420402.

Decker, S. G., and J. E. Martin, 2005: A local energetics analysis of the life cycle differences between consecutive, explosively deepening continental cyclones. *Mon. Wea. Rev.,* **133,** 295–316, doi:10.1175/MWR-2860.1.

Evans, J. L., and R. E. Hart, 2003: Objective indicators of the life cycle evolution of extratropical transition for Atlantic tropical cyclones. *Mon. Wea. Rev.,* **131,** 909–925, doi:10.1175/1520-0493(2003)131<0909:OIOTLC>2.0.CO;2.

——, J. M. Arnott, and F. Chiaromonte, 2006: Evaluation of operational model cyclone structure forecasts during extratropical transition. *Mon. Wea. Rev.,* **134,** 3054–3072, doi:10.1175/MWR3236.1.

Galarneau, T. J., L. F. Bosart, and R. S. Schumacher, 2010: Predecessor rain events ahead of tropical cyclones. *Mon. Wea. Rev.,* **138,** 3272–3297, doi:10.1175/2010MWR3243.1.

Glatt, I., A. Dörnbrack, S. C. Jones, J. H. Keller, O. Martius, A. Müller, D. H. W. Peters, and V. Wirth, 2011: Utility of Hovmöller diagrams to diagnose Rossby wave trains. *Tellus,* **63A,** 991–1006, doi:10.1111/j.1600-0870.2011.00541.x.

Grams, C. M., 2011: Quantification of the downstream impact of the extratropical transition of Typhoon Jangmi and other case studies. Ph.D. thesis, Karlsruhe Institute of Technology, 242 pp.

——, and Coauthors, 2011: The key role of diabatic processes in modifying the upper-tropospheric wave guide: A North Atlantic case-study. *Quart. J. Roy. Meteor. Soc.,* **137,** 2174–2193, doi:10.1002/qj.891.

Harr, P. A., and R. L. Elsberry, 2000: Extratropical transition of tropical cyclones over the western North Pacific. Part I: Evolution of structural characteristics during the transition process. *Mon. Wea. Rev.,* **128,** 2613–2633, doi:10.1175/1520-0493(2000)128<2613:ETOTCO>2.0.CO;2.

——, and J. M. Dea, 2009: Downstream development associated with the extratropical transition of tropical cyclones over the western North Pacific. *Mon. Wea. Rev.,* **137,** 1295–1319, doi:10.1175/2008MWR2558.1.

——, R. L. Elsberry, and T. F. Hogan, 2000: Extratropical transition of tropical cyclones over the western North Pacific. Part II: The impact of midlatitude circulation characteristics. *Mon. Wea. Rev.,* **128,** 2634–2653, doi:10.1175/1520-0493(2000)128<2634:ETOTCO>2.0.CO;2.

——, D. Anwender, and S. C. Jones, 2008: Predictability associated with the downstream impacts of the extratropical transition of tropical cyclones: Methodology and a case study of Typhoon Nabi (2005). *Mon. Wea. Rev.,* **136,** 3205–3225, doi:10.1175/2008MWR2248.1.

Hovmöller, E., 1949: The trough-and-ridge diagram. *Tellus,* **1,** 62–66, doi:10.1111/j.2153-3490.1949.tb01260.x.

Jones, S. C., and Coauthors, 2003: The extratropical transition of tropical cyclones: Forecast challenges, current understanding, and future directions. *Wea. Forecasting,* **18,** 1052–1092, doi:10.1175/1520-0434(2003)018<1052:TETOTC>2.0.CO;2.

Keller, J. H., 2012: Diagnosing the downstream impact of extratropical transition using multimodel operational ensemble prediction systems. Ph.D. thesis, Karlsruhe Institute of Technology, 246 pp.

——, S. C. Jones, J. L. Evans, and P. A. Harr, 2011: Characteristics of the TIGGE multimodel ensemble prediction system in representing forecast variability associated with extratropical transition. *Geophys. Res. Lett.,* **38,** L12802, doi:10.1029/2011GL047275.

Klein, P. M., P. A. Harr, and R. L. Elsberry, 2000: Extratropical transition of western North Pacific tropical cyclones: An overview and conceptual model of the transformation stage. *Wea. Forecasting,* **15,** 373–396, doi:10.1175/1520-0434(2000)015<0373:ETOWNP>2.0.CO;2.

——, ——, and ——, 2002: Extratropical transition of western North Pacific cyclones: Midlatitude and tropical cyclone contributions to reintensification. *Mon. Wea. Rev.,* **130,** 2240–2259, doi:10.1175/1520-0493(2002)130<2240:ETOWNP>2.0.CO;2.

Lang, S. T. K., M. Leutbecher, and S. C. Jones, 2012: Impact of perturbation methods in the ECMWF ensemble prediction system on tropical cyclone forecasts. *Quart. J. Roy. Meteor. Soc.,* **138,** 2030–2046, doi:10.1002/qj.1942.

McLay, J. G., and J. E. Martin, 2002: Surface cyclolysis in the North Pacific Ocean. Part III: Composite local energetics of tropospheric-deep cyclone decay associated with rapid surface cyclolysis. *Mon. Wea. Rev.,* **130,** 2507–2529, doi:10.1175/1520-0493(2002)130<2507:SCITNP>2.0.CO;2.

McTaggart-Cowan, R., J. R. Gyakum, and M. K. Yau, 2001: Sensitivity testing of extratropical transitions using potential vorticity inversions to modify initial conditions: Hurricane Earl case study. *Mon. Wea. Rev.,* **129,** 1617–1636, doi:10.1175/1520-0493(2001)129<1617:STOETU>2.0.CO;2.

Orlanski, I., and J. J. Katzfey, 1991: The life cycle of a cyclonic wave in the Southern Hemisphere. Part I: Eddy energy budget. *J. Atmos. Sci.,* **48,** 1972–1998, doi:10.1175/1520-0469(1991)048<1972:TLCOAC>2.0.CO;2.

——, and J. Sheldon, 1995: Stages in the energetics of baroclinic systems. *Tellus,* **47A,** 605–628, doi:10.1034/j.1600-0870.1995.00108.x.

Pantillon, F., J.-P. Chaboureau, C. Lac, and P. Mascart, 2012: On the role of a Rossby wave train during the extratropical transition of Hurricane Helene (2006). *Quart. J. Roy. Meteor. Soc.,* **139,** 370–386, doi:10.1002/qj.1974.

Riemer, M., and S. C. Jones, 2010: The downstream impact of tropical cyclones on a developing baroclinic wave in idealized scenarios of extratropical transition. *Quart. J. Roy. Meteor. Soc.,* **136,** 617–637, doi:10.1002/qj.605.

——, ——, and C. A. Davis, 2008: The impact of extratropical transition on the downstream flow: An idealized modelling study with a straight jet. *Quart. J. Roy. Meteor. Soc.,* **134,** 69–91, doi:10.1002/qj.189.

Ritchie, E. A., and R. L. Elsberry, 2003: Simulations of the extratropical transition of tropical cyclones: Contributions by the midlatitude upper-level trough to reintensification. *Mon. Wea. Rev.,* **131,** 2112–2128, doi:10.1175/1520-0493(2003)131<2112:SOTETO>2.0.CO;2.

——, and ——, 2007: Simulations of the extratropical transition of tropical cyclones: Phasing between the upper-level trough and tropical cyclones. *Mon. Wea. Rev.,* **135,** 862–876, doi:10.1175/MWR3303.1.

Scheck, L., S. C. Jones, and M. N. Juckes, 2011a: The resonant interaction of a tropical cyclone and a tropopause front in a barotropic model. Part I: Zonally oriented front. *J. Atmos. Sci.,* **68,** 405–419, doi:10.1175/2010JAS3482.1.

——, ——, and ——, 2011b: The resonant interaction of a tropical cyclone and a tropopause front in a barotropic model. Part II: Frontal waves. *J. Atmos. Sci.,* **68,** 420–429, doi:10.1175/2010JAS3483.1.

Schumacher, R. S., T. J. Galarneau Jr., and L. F. Bosart, 2011: Distant effects of a recurving tropical cyclone on rainfall in a midlatitude convective system: A high-impact predecessor rain event. *Mon. Wea. Rev.,* **139,** 650–667, doi:10.1175/2010MWR3453.1.

Torn, R. D., 2010: Diagnosis of the downstream ridging associated with extratropical transition using short-term ensemble forecasts. *J. Atmos. Sci.,* **67,** 817–833, doi:10.1175/2009JAS3093.1.